

Doppler boosting the stochastic gravitational wave background

Giulia Cusin^{1,2}, Gianmassimo Tasinato³

¹ *Department of Theoretical Physics, University of Geneva, 24 quai Ernest-Ansermet, Geneva, Switzerland*

² *Sorbonne Université, CNRS, UMR 7095, Institut d'Astrophysique de Paris, 75014 Paris, France*

³ *Physics Department, Swansea University, SA28PP, United Kingdom*

Abstract

One of the guaranteed features of the stochastic gravitational wave background (SGWB) is the presence of Doppler anisotropies induced by the motion of the detector with respect to the rest frame of the SGWB source. We point out that kinematic effects can be amplified if the SGWB is characterised by large tilts in its spectrum as a function of frequency, or by sizeable intrinsic anisotropies. Hence we examine the possibility to use Doppler effects as complementary probes of the SGWB frequency profile. For this purpose we work in multipole space, and we study the effect of kinematic modulation and aberration on the GW energy density parameter and on its angular power spectrum. We develop a Fisher forecast analysis and we discuss prospects for constraining parameters controlling kinematically induced anisotropies with future detector networks. As a case study, we apply our framework to a background component with constant slope in frequency, potentially detectable by a network of future ground-based interferometers. For this specific example, we show that a measurement of kinematic anisotropies with a network of Einstein Telescope and Cosmic Explorer will allow us to constrain the spectral shape with a precision of about 16%. We also show that, if a reconstruction of the spectral shape is done via other methods, e.g. frequency binning, a study of kinematic anisotropies can allow one to constrain our peculiar velocity with respect to the CMB frame with a precision of 30%. Finally, we identify cosmological and astrophysical scenarios where kinematic effects are enhanced in frequency ranges probed by current and future GW experiments.

1 Introduction

The detection and characterization of a stochastic gravitational wave background (SGWB) is one of the next goals for gravitational wave (GW) science. A SGWB can have astrophysical or cosmological origin, or both: see [1–3] for recent reviews. Currently, upper limits are set on the amplitude [4] of the SGWB at ground-based interferometer frequencies, and on parameters characterising the first few multipoles of its associated angular power spectrum [5, 6]. Recent tantalising hints of a signal in the nano-Hertz regime are discussed in [7].

In view of future conclusive detections, it is essential to have the best possible theoretical understanding of the properties of a SGWB. Among its guaranteed features is the presence of Doppler anisotropies induced by the motion of the detector with respect to the SGWB rest frame. In fact, the study of kinematic anisotropies in the context of stochastic backgrounds of electromagnetic radiation is an already well-developed research topic. Doppler-induced anisotropies in the spectrum of CMB fluctuations have been measured since decades [8–11], and their analysis provides interesting cosmological information [12–20]. Kinematic effects are also studied for other cosmological observables, see , see e.g. the dipole in luminosity distance of SN counts [21], or the kinematic dipole anisotropies in galaxy number counts, see e.g. [22–24].

The aim of this work is to analyse kinematic anisotropies in the SGWB, and investigate their physical consequences. In particular, we show that their properties can provide important information on the spectral dependence of the SGWB:

- In section 2 we compute how the SGWB density parameter Ω_{GW} transforms under a Doppler boost connecting the observer frame to a frame at rest with the SGWB. The boost leads to the generation of kinematic anisotropies from the rest-frame monopole, and to the modulation and aberration of existing rest-frame anisotropies. Kinematic effects are amplified if the SGWB is characterised by sizeable tilts in its spectrum as a function of frequency, or by intrinsic anisotropies. Consequently, Doppler effects offer complementary probes of the SGWB frequency profile, as well as of its rest-frame anisotropies.
- In section 3 we identify set-ups where kinematic effects can be amplified in frequency ranges probed by GW experiments, thanks to transient enhancements of the tilt of the SGWB spectrum. For cosmological background components, such amplifications can occur when tensor modes are sourced at second order by scalar spectra with pronounced peaks, as in inflationary models producing primordial black holes. For an astrophysical background, scenarios with a rapid after merger drop of the density parameter can potentially lead to a local enhancement of kinematic anisotropies.
- In section 4 we discuss applications of our results, elaborating prospects of detection of kinematically-induced effects. We investigate constraints on the slope of the SGWB spectrum associated with measurements of boost induced anisotropies. We develop a multipolar decomposition of the SGWB spectrum including Doppler effects. We show how the latter depend on the tilt of the spectrum, and how they affect correlation functions. We develop Fisher forecasts for computing the signal-to-noise ratio relative to parameters controlling kinematically induced anisotropies. We then apply our general formulas to the

idealised case of an astrophysical background with constant slope in frequency, detectable by a network of future interferometers. For this specific example, we show that a measurement of kinematic anisotropies allows us to constrain the spectral shape of the SGWB with a precision of about 16%. We also show that, if a reconstruction of the spectral shape is done via other methods, e.g. frequency binning, a study of kinematic anisotropies can allow one to constrain our peculiar velocity with respect to the CMB frame with a precision of 30%.

- We present our conclusions and future directions of our study in section 5, which is followed by a technical appendix A.

2 Transforming the GW density parameter under boosts

In this section we discuss how the GW density parameter Ω_{GW} transforms under a Doppler boost connecting two frames moving with relative velocity \mathbf{v} . In subsection 2.1 we obtain the general formulas for boost transformations. In subsection 2.2 we apply them to a case where the GW density parameter Ω_{GW} is isotropic in the rest frame, and we demonstrate that kinematic anisotropies are induced by the boost¹. In subsection 2.3 we discuss a more general scenario where the GW density parameter Ω_{GW} is anisotropic in the rest frame. We show how kinematic effects, besides inducing new anisotropies, lead to modulation and aberration of existing ones. The size of the Doppler-induced effects are enhanced if the SGWB spectrum has large tilts in frequency. This property suggests an independent way for probing the frequency dependence of the spectrum. See also [26] for an analysis of the kinematic dipole of the SGWB, with applications to the case of cosmic string sources.

2.1 The general formulas

Let us consider two sets of observers in an unperturbed FLRW universe. The first observer, called \mathcal{S}' , is comoving with the SGWB rest frame. The second one, \mathcal{S} , moves with constant velocity \mathbf{v} with respect to \mathcal{S}' . Primes indicate rest-frame quantities; vectors with a hat are unit vectors. The boost connects the SGWB density parameters in the two frames \mathcal{S}' and \mathcal{S} . We identify two qualitatively different effects of the observer motion on the SGWB sky map²:

1. The generation of higher multipole anisotropies from lower multipole ones.
2. The modulation and aberration of the intensity of existing anisotropies. This leads to a remapping of the intensity map/Stokes parameters on the sky.

We use the approach of [27] to determine how quantities change from one frame to the other (see also [13, 18, 28]). We denote with f' the frequency of the GW in the SGWB rest frame, and with $\hat{\mathbf{n}}'$ the unit vector denoting its direction. The frequency f in the system in motion is

¹Part of the contents of these two subsections can be found in [25].

²While we investigate these effects in the case of the SGWB, it is worth to point out that they are already well-known in the CMB literature.

related to f' by a Lorentz transformation reading

$$f = \frac{\sqrt{1 - \beta^2}}{1 - \beta \xi} f', \quad (2.1)$$

where $\mathbf{v} = \beta \hat{\mathbf{v}}$ denotes the relative velocity of the two frames: we have $\beta = v$ in units with $c = 1$. The unit vector $\hat{\mathbf{v}}$ corresponds to the direction of the relative motion between the two frames. We introduce the convenient quantity

$$\xi = \hat{\mathbf{n}} \cdot \hat{\mathbf{v}}, \quad (2.2)$$

parametrising the relative angle between $\hat{\mathbf{n}}$ and $\hat{\mathbf{v}}$. We re-express equation (2.1) as

$$f = \mathcal{D} f', \quad (2.3)$$

with

$$\mathcal{D} = \frac{\sqrt{1 - \beta^2}}{1 - \beta \xi}. \quad (2.4)$$

The directions of GW propagation in the two frames \mathcal{S}' and \mathcal{S} are related by the aberration equation of special relativity [11]

$$\hat{\mathbf{n}}' = \frac{\hat{\mathbf{n}} + \hat{\mathbf{v}} [(\gamma - 1) \xi - \gamma \beta]}{\gamma (1 - \beta \xi)}, \quad (2.5)$$

with

$$\gamma = \frac{1}{\sqrt{1 - \beta^2}}. \quad (2.6)$$

In order to compute how the GW energy density changes under boosts, we make use of the GW distribution function, denoted here with $\Delta'(f', \hat{\mathbf{n}}')$. We assume it only depends on the frequency f' and on the GW direction $\hat{\mathbf{n}}'$ in the SGWB rest frame. We express the number of gravitons for unit of phase space in the rest-frame \mathcal{S}' as:

$$dN' = \Delta'(f', \hat{\mathbf{n}}') f'^2 df' d^2 \hat{\mathbf{n}}' dV', \quad (2.7)$$

where dV' corresponds to the infinitesimal volume containing gravitons with propagation vector $\hat{\mathbf{n}}'$ in the element of measure $df' d^2 \hat{\mathbf{n}}'$. The combination $f'^2 df' d^2 \hat{\mathbf{n}}' dV'$ is invariant under boosts. In fact, the relations $f' = \mathcal{D}^{-1} f$, $d^2 \hat{\mathbf{n}}' = \mathcal{D}^2 d^2 \hat{\mathbf{n}}$, $dV' = \mathcal{D} dV$ hold (see [18, 27]). On the other hand, the number of gravitons (2.7) is independent of the frame, and $dN' = dN$. Hence [28]

$$\Delta'(f', \hat{\mathbf{n}}') = \Delta(f, \hat{\mathbf{n}}). \quad (2.8)$$

The GW distribution function Δ can be used to define the energy density of GW in the rest frame as energy per unit volume and unit solid angle:

$$d\rho'_{\text{GW}}(f', \hat{\mathbf{n}}') = \frac{f' dN'}{d^2 \hat{\mathbf{n}}' dV'} = \Delta'(f', \hat{\mathbf{n}}') f'^3 df'. \quad (2.9)$$

We then express the GW density parameter $\Omega'_{\text{GW}}(\omega', \hat{\mathbf{n}}' \hat{\mathbf{v}})$ in the rest frame \mathcal{S}' as

$$\Omega'_{\text{GW}}(f', \hat{\mathbf{n}}') \equiv \frac{1}{\rho_c} \frac{d\rho'_{\text{GW}}}{d \ln f'} = \frac{3\pi f'^4}{2 H_0^2 M_{\text{Pl}}^2} \Delta'(f', \hat{\mathbf{n}}'). \quad (2.10)$$

Using eq (2.8), we find the equality

$$\Omega_{\text{GW}}(f, \hat{\mathbf{n}}) = \left(\frac{f}{f'}\right)^4 \Omega'_{\text{GW}}(f', \hat{\mathbf{n}}'). \quad (2.11)$$

Collecting the results so far, we find that the GW density parameter in the moving frame \mathcal{S} is related with the corresponding quantity in the frame \mathcal{S}' at rest through the formula

$$\boxed{\Omega_{\text{GW}}(f, \hat{\mathbf{n}}) = \mathcal{D}^4 \Omega'_{\text{GW}} \left(\mathcal{D}^{-1} f, \frac{\hat{\mathbf{n}} + \hat{\mathbf{v}} [(\gamma - 1) \xi - \gamma \beta]}{\gamma (1 - \beta \xi)} \right)} \quad (2.12)$$

with \mathcal{D} , γ and ξ given respectively in eqs (2.4), (2.6), (2.2). The previous formula is completely general and valid for any values of $0 \leq \beta \leq 1$. On the other hand, the parameter β is usually small: for example, for cosmological backgrounds, CMB suggests that $\beta \simeq 1.23 \times 10^{-3}$. Under the assumption of small β , we Taylor expand eq (2.12) in β , and analyse two cases.

2.2 First example: the SGWB is isotropic in the rest frame

We assume that the GW density parameter in the rest frame \mathcal{S}' is isotropic, and independent of $\hat{\mathbf{n}}'$: $\Omega'_{\text{GW}} = \Omega'_{\text{GW}}(f')$. It is then straightforward to expand eq (2.12) up to the quadrupole (and also beyond if needed, see section 4). Taking the notation from CMB physics, we introduce the tilts of the SGWB spectrum as

$$n_{\Omega}(f) = \frac{d \ln \Omega'_{\text{GW}}(f)}{d \ln f}, \quad (2.13)$$

$$\alpha_{\Omega}(f) = \frac{d n_{\Omega}(f)}{d \ln f}. \quad (2.14)$$

These spectral tilts play an important role in our analysis. Expanding (2.12) in powers of β , and limiting the expansion to order β^2 – in fact we are assuming that β is small – we find that the GW density parameter in the moving frame \mathcal{S} receives a kinematic modulation of the monopole. Moreover, a kinematic dipole and a kinematic quadrupole are generated by boost effects:

$$\Omega_{\text{GW}}(f, \hat{\mathbf{n}}) = \Omega'_{\text{GW}}(f) \left[1 + M(f) + \xi D(f) + \left(\xi^2 - \frac{1}{3} \right) Q(f) \right], \quad (2.15)$$

where remember we define $\xi = \hat{\mathbf{n}} \cdot \hat{\mathbf{v}}$. The frequency-dependent coefficients

$$M(f) = \frac{\beta^2}{6} (8 + n_{\Omega} (n_{\Omega} - 6) + \alpha_{\Omega}), \quad (2.16)$$

$$D(f) = \beta (4 - n_{\Omega}), \quad (2.17)$$

$$Q(f) = \beta^2 \left(10 - \frac{9n_{\Omega}}{2} + \frac{n_{\Omega}^2}{2} + \frac{\alpha_{\Omega}}{2} \right), \quad (2.18)$$

indicate respectively the monopole, dipole, quadrupole boost contributions; from now on we understand for simplicity the frequency dependence of the spectral tilts.

The quantities within brackets in the expressions (2.16), (2.17), (2.18) depend on numerical coefficients, as well as on the spectral tilts n_Ω and α_Ω , as defined in eqs (2.13), (2.14). Notice that when the spectral tilts are of at least of order one, they give a sizeable contributions to the kinetically induced effects of eqs. (2.16)-(2.18). Hence the slope of the spectrum influences the kinematic anisotropies through n_Ω , α_Ω : in scenarios where these quantities are large, boost effects are amplified, and can be used to probe the slope of the spectrum.

The monopole contribution $M(f)$ receives a modulation of its intensity at order β^2 in the expansion. See [29] for a study of this effect in the context of the CMB, and more in general section 2 of [11] for comparing our formulas to their analog in a CMB context, with the frequency-dependence of the CMB intensity taking the place of what for us is the frequency-dependence of Ω_{GW} . The dipole contribution (2.17) is the only one starting already at order β^1 in the expansion, and it is typically the largest boost-induced modulation effect.

While our expression (2.15) is built in terms of combinations of $\xi = \hat{\mathbf{n}} \cdot \hat{\mathbf{v}}$, it is also straightforward to convert it in spherical harmonics. We choose for simplicity $\hat{\mathbf{v}}$ along the z -direction, and parameterize $\hat{\mathbf{n}} = (\sin \theta \cos \varphi, \sin \theta \sin \varphi, \cos \theta)$. Then we can rewrite (2.15) in terms of spherical harmonics $Y_{\ell m}(\theta, \varphi)$ as

$$\Omega_{\text{GW}}(f, \hat{\mathbf{n}}) = \sqrt{4\pi} \Omega'_{\text{GW}}(f) \left[(1 + M(f)) Y_{00}(\theta, \varphi) + \frac{D(f)}{\sqrt{3}} Y_{10}(\theta, \varphi) + \frac{2Q(f)}{\sqrt{45}} Y_{20}(\theta, \varphi) \right]. \quad (2.19)$$

Choosing $\hat{\mathbf{v}}$ in the z -direction implies that only the $m = 0$ harmonics are induced by the boosts – more general choices induce other harmonics as well, and are related to the previous formula by a spatial rotation (see section 4, especially footnote 9.).

2.3 Second example: the SGWB is anisotropic in the rest frame

Doppler boosts cause aberration effects that change the map distribution of rest-frame anisotropies in the sky. We investigate this effect in our second example, where we do not assume that Ω'_{GW} is isotropic in the rest frame \mathcal{S}' . For simplicity we assume a factorisable Ansatz [30]:

$$\Omega'_{\text{GW}}(f', \hat{\mathbf{n}}') = \Omega'(f') \Phi'(\hat{\mathbf{n}}'). \quad (2.20)$$

We now derive the resulting $\Omega_{\text{GW}}(f, \hat{\mathbf{n}})$ in the moving frame \mathcal{S} . We will find that the quantity $\Omega_{\text{GW}}(f, \hat{\mathbf{n}})$ in the moving frame \mathcal{S} does not obey any more a factorisable Ansatz as in eq (2.20). In fact, using eq (2.12) we express Ω_{GW} as (recall $\xi = \hat{\mathbf{v}} \cdot \hat{\mathbf{n}}$)

$$\Omega_{\text{GW}}(f, \hat{\mathbf{n}}) = [\mathcal{D}^4 \Omega'(\mathcal{D}^{-1} f)] \times \left[\Phi' \left(\frac{\hat{\mathbf{n}} + \hat{\mathbf{v}} [(\gamma - 1) \xi - \gamma \beta]}{\gamma (1 - \beta \xi)} \right) \right]. \quad (2.21)$$

Expanding up to first order β^1 , we get

$$\Omega_{\text{GW}}(f, \hat{\mathbf{n}}) = \Omega'_{\text{GW}}(f, \hat{\mathbf{n}}) \left[1 + \beta \xi (4 - n_\Omega) - \beta \xi_{,i} (\ln \Omega'_{\text{GW}})_{,i} \right], \quad (2.22)$$

where we denote with a comma the covariant derivative, $\nabla_i \xi = \xi_{,i}$, and we use the identity $\xi_{,i} = \hat{\mathbf{v}}_i - \xi \hat{\mathbf{n}}_i$. The second term in the parenthesis of (2.22) is a kinematic modulation of the rest-frame Ω'_{GW} ; the third term is due to kinematic aberration.

We can also directly expand eq (2.21) in powers of β , and use a spherical harmonic decomposition so to understand in a more transparent way the physical implication of a Doppler boost. We will carry on a more general analysis of these topics in section 4. To acquire familiarity with physical consequences of boosting rest-frame anisotropies, here we present kinematic effects up to the quadrupole $\ell = 2$ expanding at second order in β .

We express the rest-frame function $\Phi'(\hat{\mathbf{n}}')$ appearing in eq (2.20) as

$$\Phi'(\hat{\mathbf{n}}') = \sqrt{4\pi} \sum_{\ell=0}^2 \sum_{m=-\ell}^{\ell} \Phi'_{\ell m} Y_{\ell m}(\theta, \varphi), \quad (2.23)$$

where $\Phi'_{\ell m}$ are the constant coefficients of the spherical harmonic decomposition in the rest frame \mathcal{S}' of the SGWB. They are frequency-independent given the factorization hypothesis of (2.20). We assume a unit monopole coefficient $\Phi'_{00} = 1$, factorising it in the overall frequency-dependent factor. We implement this decomposition in eq (2.21), expanding up to order β^2 . As done in the previous section, we assume that $\hat{\mathbf{v}}$ points towards the e_z direction. We expand the GW density parameter up to the quadrupole in the basis of spherical harmonics, finding

$$\Omega_{\text{GW}}(f, \hat{\mathbf{n}}) = \sqrt{4\pi} \Omega'(f) \sum_{\ell=0}^2 \sum_{m=-\ell}^{\ell} \Phi_{\ell m}(f) Y_{\ell m}(\theta, \varphi), \quad (2.24)$$

with the following non-vanishing anisotropy coefficients

$$\Phi_{00} = 1 + \frac{\beta}{\sqrt{3}} (2 - n_{\Omega}) \Phi'_{10} + \frac{\beta^2}{6} [8 + n_{\Omega} (n_{\Omega} - 6) + \alpha_{\Omega}] + \frac{\sqrt{5} \beta^2}{12} [50 + (n_{\Omega} - 21)n_{\Omega} + \alpha_{\Omega}] \Phi'_{20}, \quad (2.25)$$

$$\Phi_{10} = \Phi'_{10} + \frac{\beta}{\sqrt{3}} (4 - n_{\Omega}) + \frac{\sqrt{5} \beta}{\sqrt{12}} (n_{\Omega} - 10) \Phi'_{20} + \frac{\beta^2}{2} (3n_{\Omega} - 14) \Phi'_{10}, \quad (2.26)$$

$$\Phi_{20} = \Phi'_{20} + \frac{2\beta}{\sqrt{15}} (5 - n_{\Omega}) \Phi'_{10} + \frac{\beta^2}{3\sqrt{5}} (20 - 9n_{\Omega} + n_{\Omega}^2 + \alpha_{\Omega}) - \frac{\beta^2}{6} [80 + (n_{\Omega} - 24)n_{\Omega} + \alpha_{\Omega}] \Phi'_{20}. \quad (2.27)$$

The previous expressions ³ have interesting properties:

- The monopole Φ_{00} in the moving frame is modulated by boost induced contributions at order β^2 in the expansion, as well as new parts inherited from the rest-frame dipole Φ'_{10} and quadrupole Φ'_{20} . Notice that there is a contribution at order β^1 , induced by the intrinsic dipole Φ'_{10} , which is generally the largest in size given our hypothesis of a small- β expansion.

³In general, the Taylor expansions we consider always converge to the formula in eq (2.12) we started from, so they are mathematically consistent. However, if the tilts of the SGWB are too large, there is the risk that the terms we neglect in the expansions are of the same order than the ones we consider, hence our truncations can be physically misleading. In what follows, we will consider our formulas to be valid in regimes where the terms we neglect in the Taylor expansions are hierarchically smaller than the contributions we include.

- Both the dipole Φ_{10} and quadrupole Φ_{20} receive kinematic modulations of their rest-frame amplitudes, as well as a kinematic aberration depending on the amplitude of the rest-frame quantities Φ'_{10} and Φ'_{20} . Besides a kinematic modulation at order β^2 to the dipole, new aberration effects arise at order β^1 , which depend on the size of existing rest-frame anisotropies.

Hence a Doppler boost introduces kinematic aberrations that mix different orders in a multipole expansion. For example, at order β^1 , the moving frame dipole coefficient Φ_{10} receives contributions from the rest-frame quadrupole Φ'_{20} , and the moving frame quadrupole coefficient Φ_{20} receives contributions from the rest-frame dipole Φ'_{10} . We will meet again and make use of this phenomenon in section 4. The formulas we derived in section 2.2 and this section 2.3, starting from the general result in eq (2.12), go beyond what previously done in the literature, for example by considering a Taylor expansion beyond the linear order in β (see e.g. [26] for linear order expressions), and including the effects of intrinsic anisotropies, not discussed in [25].

The modulation and aberrations effects can be amplified in models with an enhanced slope of the GW spectrum in certain range of frequencies, and/or in scenarios with intrinsic large anisotropies in the rest frame. This suggests that Doppler effects can be used as a complementary probe of the SGWB frequency profile, as well as of its intrinsic rest-frame anisotropies. We elaborate on this topic in what comes next.

3 Kinematic anisotropies and SGWB scenarios

In this section we explore cosmological and astrophysical scenarios where our previous findings can be applied. We are especially interested in theoretically identifying set-ups where kinematic effects can be amplified in frequency ranges probed by GW experiments, thanks to enhancements of the tilts n_Ω , α_Ω of the SGWB spectrum at particular frequencies. We focus on the SGWB from inflation (subsection 3.1) and from astrophysical sources (subsection 3.2).

3.1 Primordial SGWB from the early universe

In analogy to what happens for the CMB, we expect also the SGWB to be characterized by kinematic anisotropies due to the motion of the solar system with respect to the cosmic rest frame with velocity $\beta = 1.23 \times 10^{-3}$. Several early universe models predict rich slopes in frequency for the spectrum of Ω_{GW} which can be probed at interferometer scales (see e.g. [31] for a study in the context of LISA). In these models, spectral tilts can become large enough to compensate for the smallness of β in our Taylor expansion.

Focussing on a frequency range that can be probed with space-based or ground-based interferometers, one finds (see e.g. [3]):

$$h_0^2 \Omega_{\text{GW}}(f) = 6.73 \times 10^{-7} \mathcal{P}_T(f), \quad (3.1)$$

which shows that $\Omega_{\text{GW}}(f)$ is proportional to the primordial isotropic spectrum of tensor modes, defined as

$$\mathcal{P}_T(f) = \frac{k^3}{2\pi} \langle h_{ij}^2 \rangle',$$

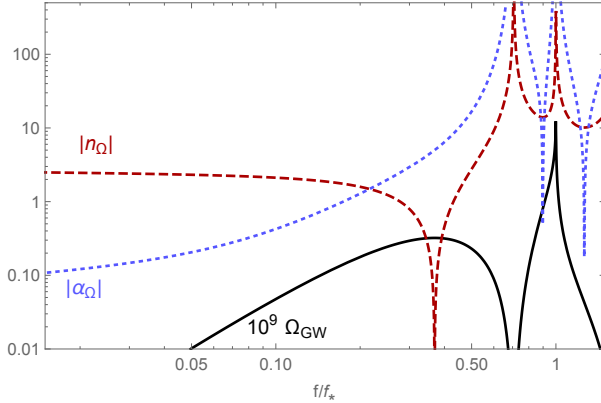


Figure 1: Plot of the GW density parameter Ω_{GW} obtained from the scalar spectrum of (3.2) with width $\Delta = 0.2$. We also represent the absolute value of its tilts n_Ω and α_Ω . The tilts become large at the location of features of the spectrum.

where a prime indicates 2-point correlators understanding the momentum-conserving Dirac delta. For scale-invariant and power-law primordial tensor spectra with constant slope (which can be relatively large and blue-tilted in models of supersolid inflation, see e.g. [32–34]), it is simple to obtain the tilts of the spectrum using eq (2.13) and (2.14), and to compute the expressions for the Doppler anisotropies.

We analyze here a slightly less straightforward example, so to explore physically well-motivated situations where the frequency-dependence of the spectrum is richer. We consider a primordial SGWB sourced at second order in perturbations from scalar fluctuations enhanced at small scales, a subject first explored in [35–41]. These scenarios arise frequently in models leading to primordial black hole production, see e.g. [42, 43] for recent reviews. Such source can induce a rich frequency dependence in the tensor spectrum, particularly when the width of the scalar spectrum is small and centered at a characteristic frequency f_\star (see e.g. [44, 45]).

For example, we can parameterise the scalar spectrum \mathcal{P}_ψ in terms of log-normal Gaussian peak in frequency, as

$$\mathcal{P}_\psi(f) = \frac{\mathcal{A}}{\sqrt{2\pi}\Delta} \exp\left\{-\frac{[\ln(f/f_\star)]^2}{2\Delta^2}\right\}. \quad (3.2)$$

Such Ansatz leads to fully analytical formulas for Ω_{GW} , as shown in [46] building on the works of [40, 41, 44, 45, 47, 48]. In eq (3.2), \mathcal{A} is the amplitude of the peak, Δ its width, and f_\star a characteristic frequency. The resulting GW spectrum has a rich and steep profile in frequency if $\Delta \ll f_\star$. We represent the profile of the induced Ω_{GW} in Fig 1, using the analytic results of [46]. We also plot the absolute value of the parameters n_Ω and α_Ω , as defined in (2.13), (2.14). A scalar spectrum with a single pronounced peak as the one of eq (3.2) can also be obtained in multifield inflation, see for example [49].

In fact, in the limit of thin peak $\Delta \ll f_\star$, the features of Ω_{GW} can be analytically understood (see e.g. [40, 44, 45]). The GW spectrum starts increasing as f^2 from small towards large frequencies. It then shows a rapid drop in power and a zero at frequencies of order $f/f_\star = \sqrt{2/3}$.

A resonance ⁴ then produces a pronounced peak, occurring at frequency $f/f_\star = 2/\sqrt{3}$. It then definitely drops and it vanishes at frequencies $f/f_\star > 2$, since, working at second order in perturbations, momentum conservation does not allow to generate tensors whose momenta are larger than twice the scalar momentum.

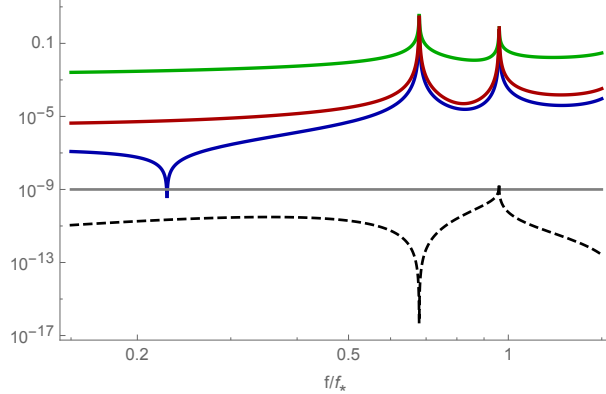


Figure 2: Representation of the relative contributions to eq (2.15) for the system GW density parameter represented in Fig 1. We choose the CMB value for $\beta = 1.23 \times 10^{-3}$. Blue is the monopole; Green is the dipole divided by β ; Red is the quadrupole divided by β^2 . Below the grey line, for reference, we include the shape profile of the original Ω_{GW} in arbitrary units. Notice that the dipole contribution, starting at order β^1 , is much larger than the others, and can be up to two orders of magnitude larger than β within the frequency range where features in the spectrum occur.

Let us assume that the primordial anisotropies in the rest-frame \mathcal{S}' are negligible, so to work in the set-up of section 2.2. Due to the large absolute values of the tilt parameters n_Ω , α_Ω we expect large induced kinematic anisotropies at least in the specific frequency range $\sqrt{2/3} \leq f/f_\star \leq 2$. The amplitude of the kinematic contributions to the monopole, dipole, and quadrupole of the SGWB amplitude in the moving frame \mathcal{S} is controlled by the functions $M(f)$, $D(f)$, $Q(f)$ introduced in eq (2.15). In figure 2 we plot these quantities as a function of frequency, showing that they are indeed enhanced in the expected frequency interval: the dipole contribution is the dominant one since it is weighted by a single power β^1 of the expansion parameter. In particular, a pronounced amplification of kinematic anisotropies occurs at the position of the first dip of the spectrum, around $f/f_\star = \sqrt{2/3}$.

We should now reconsider footnote 3. Given that the spectral tilts become large where the spectrum has features – see Fig 1 – we might ask whether the expansion in powers of β is consistent in this context. In particular we want to check whether higher order contributions to the kinematic anisotropies can turn larger than the ones we included, thus invalidating our formulas truncated at second order in a β expansion. We discuss this issue in the technical Appendix B, where we show that higher order corrections in a β expansion are hierarchically smaller, hence the results plotted in Fig 2 are robust.

It would be interesting to explore whether a detection of kinematically induced anisotropies is possible for these scenarios, and whether it can complement direct measurements of the slope of the spectrum (see e.g. [50–52] for methods and forecasts). This possibility would allow one

⁴In realistic examples, we expect the sharp peak at the resonance position to be smoothed out [40], so we will not consider the enhancement of kinematic effects occurring precisely at the resonance frequency $f/f_\star = 2/\sqrt{3}$.

to better characterize the spectral profile of the SGWB. We discuss first steps towards this aim in section 4. We notice that while we focussed on the consequences of a single peak in scalar fluctuations, there are more complex models with multiple peaks, steps in the inflationary potential, or multifield inflationary scenarios where even richer features occur in the spectrum as function of frequency – see for example [53–56].

Until now, we assumed that the SGWB spectrum is perfectly isotropic in the rest frame. On the other hand, anisotropies are expected, both of primordial origin, or induced by propagation effects from the early universe to today: see e.g. [57–65]. For example, sizeable intrinsic quadrupolar anisotropies can be produced in scenarios with large tensor non-Gaussianity, see e.g. [33, 34, 66–69]. It would be interesting to study effects of kinematic aberration on these intrinsic anisotropies, given that they can be induced already at order β^1 (see section 2.3) and might then be enhanced in frequency ranges where the spectrum has enhanced tilts.

Measurements of kinematic dipolar anisotropies have also been proposed as a method to detect the chirality of a cosmological SGWB with planar interferometers, see [70, 71]. Our analysis can be extended to study how parity violating effects can influence Doppler-induced modulations and aberrations at higher order in a multipole expansion. We leave the exploration of these topics to future studies, as well as an analysis of the impact of black hole binaries on the detection of the primordial background [72].

3.2 Astrophysical SGWB

The astrophysical stochastic gravitational-wave background (AGWB) is generated by the superposition of signals from various resolved and unresolved astrophysical sources from the onset of stellar activity until today see e.g. [1, 73, 74]. The AGWB from binary black hole coalescence (BH) is expected to be dominant in the Hz band and below [75], and may become a source of confusion noise for some of the other types of sources.

The detection of the binary neutron star (NS) coalescence by the LIGO/Virgo network [76], and the estimated rate R of mergers in the local Universe, which is of order $R = 920_{-790}^{+2220} \text{Gpc}^{-3} \text{yr}^{-1}$ [77], lead to the conclusion that these sources may have a comparable contribution to the AGWB relative to binary BHs [78]. We may therefore expect that their contribution to the anisotropies of the AGWB is also important.

It is important to stress that the AGWB in the mHz and Hz band (accessible respectively by space and ground-based interferometers) is very different in nature. In the mHz band, we are sensitive to the inspiralling phase of the evolution of binary system of (solar mass) compact objects. The duration of the inspiralling phase is long with respect to human time scales, hence the background in the mHz band is irreducible. In the Hz band, however, we detect the very final phase of the evolution of binary systems of compact objects: mergers are well separated in the time-domain, with almost no overlap in time ⁵.

We represent in Fig. 3 the evolution of the energy density with frequency for the astrophysical model used as a reference model in [79, 80]. In the infrared side of the spectrum, the scaling

⁵In other words, with an instrument of very high sensitivity, these events are detectable individually with a catalogue approach. For this reason the background in the Hz band is not irreducible (at least as long as we focus on black hole merger contributions).

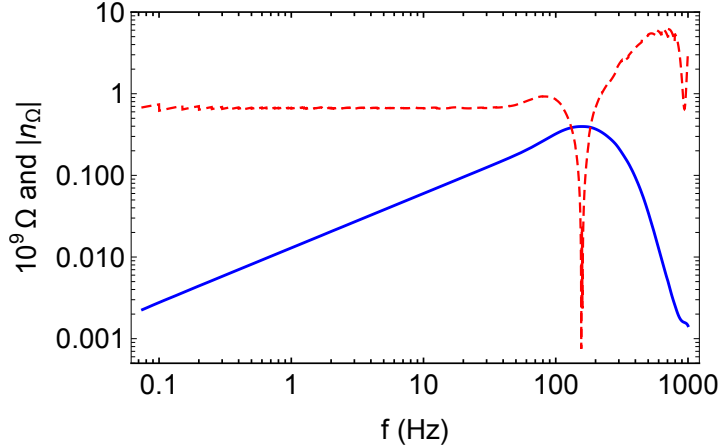


Figure 3: Energy density parameter as function of frequency for AGWB dominated by black hole mergers, compared with the corresponding spectral index as function of frequency (red dashed line). We choose the astrophysical model of [79, 80] for the source population. Notice the rapid drop in frequencies at the coalescence stage of the BH population, leading to an increase of the tilt of the spectrum of almost an order of magnitude.

with frequency follows the $\Omega_{\text{GW}} \propto f^{2/3}$ rule dictated by the Einstein quadrupole formula which captures the dynamics of the inspiralling phase. The peak in the Hz band is due to GW emission during the merger phase. While this qualitative behaviour is universal, the width of the peak and how fast it decays depends on the details of the underlying model for mass and redshift distribution of sources. For example, in the unrealistic scenario in which all coalescing binaries have the same mass M and are located at the same distance D , the spectrum has a rapid drop in frequency at a given $f = f_{\text{drop}}(M, D)$, because the sources of AGWB become ineffective at frequencies larger than f_{drop} . In this case, the tilt of the spectrum can be large at frequencies around f_{drop} , enhancing the size of kinematic effects on the AGWB anisotropies.

Traditionally, the energy density of the AGWB has been modeled and parameterized under the assumption that both our universe and the distribution of sources are homogeneous and isotropic (see e.g. Refs. [1, 75]). This is a rather crude approximation: GW sources are located in galaxies embedded in the cosmic web; moreover, once a GW signal is emitted, it is deflected by the presence of massive structures, such as galaxies and compact objects. It follows that the energy flux from all astrophysical sources has a stochastic, anisotropic dependence on direction.

The first prediction of the AGWB angular power spectrum was presented in [81, 82] following the methods developed in Refs. [83, 84]. This framework is flexible and splits the cosmological large-scale structure and sub-galactic scales so that it can be applied to any source contributions and to any frequency band. The astrophysical dependence of the angular power spectrum on the detail of the underlying astrophysical model has been studied in [26, 79, 80, 85, 86] and different formal aspects of the derivation of anisotropies and their interpretation are discussed in [58, 74, 87, 88, 90]. The angular power spectrum on large angular scales is characterized by the typical decay of the galaxy correlation function as a function of multipoles ℓ , i.e. $C_\ell \propto (\ell + 1)^{-1}$. This is not surprising as GW sources are a biased tracer of the underlying galaxy distributions and clustering is the dominant contribution to the energy density anisotropy. This implies that

in the multiple expansion (2.25), which relates boosted and unboosted multipoles, one gets $\Phi'_\ell \sim \sqrt{(\ell-1)/\ell} \Phi'_{\ell-1}$. Hence, the intrinsic dipole and quadrupole anisotropies are typically of the same size. In the next section we will learn that the effect of a boost is to generate an off-diagonal structure in the correlation matrix of the energy density: at a given order β^n in an expansion in the boost velocities, we find correlations between multipoles separated by $\pm n$ in their multipole indexes.

Based on the recent observations of merging black holes and neutron star binaries by the Advanced LIGO and Advanced Virgo detectors, [4], we expect that the stochastic background from unresolved stellar-mass compact binaries may be detected within a few years of operation of the extended LIGO-Virgo network. Its anisotropic component is constrained by LIGO/Virgo observations up to $\ell = 4$ [91], resulting in upper limits on the amplitude of the dimensionless energy density per units of logarithmic frequency in the range $\Omega_{\text{GW}}(f = 25\text{Hz}, \Theta) < 0.64 - 2.47 \times 10^{-8} \text{ sr}^{-1}$ for a population of merging binary compact objects, where Θ denotes the angular dependence. The updated analysis [6] – including also Virgo data – improves these bounds by factors of 2.8 – 3.8. See also [92] for a proposal of developing future large baseline interferometers for reaching higher values of multipoles ℓ .

The study of the cross correlations with electromagnetic observables provides complementary information and might improve the signal to noise of the anisotropic searches [79, 90, 93]. Moreover, by cross-correlating the GW background (which collects contribution from sources at all redshifts along the line of sight) with EM observables at a given redshift (such as galaxy number counts), we can study a tomographic reconstruction of the redshift distribution of sources [79, 81, 89, 90, 93].

We close this section with a brief comment on the contribution to the AGWB from coalescences of galactic sources – see e.g. [94, 95] for recent detailed studies. In this case, the AGWB is expected to be extremely anisotropic (see [30] for an early forecast of detection of anisotropies), and the size of the peculiar velocity β with respect to the solar system frame is *not* necessarily the same as the cosmological one $\beta = 1.23 \times 10^{-3}$ we considered above. It would be interesting to understand whether Doppler effects can be used for disentangling and characterizing its properties. We leave a study of this topic to future work.

4 Prospects of detection

In the previous sections we identified two physically relevant implications of Doppler boosting a SGWB. First, the generation of kinematic anisotropies in the moving frame \mathcal{S} of a detector starting from the monopole in the rest frame \mathcal{S}' of the emitter. Second, the modulation and aberration of anisotropies in frame \mathcal{S} starting from anisotropies in frame \mathcal{S}' . All these effects depend on both the absolute value of the velocity β and on the frequency slope of the emitted GW spectrum. In particular, non-stochastic anisotropies are a modulation of the monopole, while stochastic anisotropies are a modulation (and aberration) of intrinsic anisotropies. The latter are typically suppressed with respect to the intrinsic anisotropies, unless the spectral index of the SGWB profile is very large, hence $\beta n_\Omega \sim 1$. In this section we forecast prospects

of detecting kinematic effects using both the information contained in the stochastic and non-stochastic anisotropies ⁶.

The fact that non-stochastic anisotropies depend on the spectral frequency shape and on the relative velocity with respect the CMB rest frame has two interesting applications. First, a measurement of kinematic anisotropies (and in particular of the kinematic dipole) can provide us with a complementary way to probe the frequency-dependence of the SGWB spectrum. This can be useful in scenarios where an extragalactic and a galactic background components are overlapped, making it difficult a spectral shape reconstruction via frequency binning ⁷. In such a situation, measuring the kinematic dipole helps in distinguishing the backgrounds, since the extragalactic contributions to the SGWB are expected to have different intrinsic velocities with respect to galactic ones. Second, if a spectral reconstruction is possible via binning, then, out of kinematic anisotropies, one can extract information on the value of β , in a similar (but complementary) way of what done in CMB studies.

In this section we forecast the precision associated with measurements of boost-induced anisotropies, given a detector network. In particular, we focus on the possibility of using the Doppler effect for measuring the tilt n_Ω of the SGWB frequency spectrum, and the absolute value of the velocity β assuming that the spectral shape is reconstructed from the monopole. For the forecasts, we use standard textbook methods [97] and we provide analytical expressions for the SNR of boost-induced anisotropies and for the variance associated with uncertainties on n_Ω and β . As an illustration, we consider a simple case study: an astrophysical background in the Hz (ground-based) band, measured with a detector network given by Einstein Telescope (ET) and Cosmic Explorer (CE) plus a *futuristic* variation of this set-up where both the instruments have an improved strain sensitivity.

4.1 The multipolar decomposition

We now propose a multipolar expansion of the GW density parameters which allows one to study the impact of boost effects on its correlation function. We derive formulas which are valid for any multipole ℓ ; however, for simplicity we include only effects up to first order β^1 in our Taylor expansion. In this sense, we go beyond what we did in section 2, although we limit to first order in β (see also [18] for a more complete treatment suited for CMB).

We assume that the density parameter can be factorized into a frequency and a direction dependent component. In particular, the density parameter Ω'_{GW} in the rest frame \mathcal{S}' is then assumed to have the same form of eq (2.20):

$$\Omega'_{\text{GW}}(f', \hat{\mathbf{n}}') = \Omega'(f')\Phi'(\hat{\mathbf{n}}'). \quad (4.1)$$

In order to study correlations among the values of Ω_{GW} along different directions, we find convenient to split the moving-frame GW density parameter in two parts as (see also [98,99] for

⁶However, in most cases – like the vanilla example we will use for illustration – the stochastic part of the spectrum is not measurable, and one should focus on the non-stochastic part of the SGWB.

⁷A concrete example is the galactic noise contribution to a SGWB signal in the lower part of the LISA frequency band, see e.g. [96].

a similar analysis in the CMB context)

$$\Omega_{\text{GW}}(f, \mathbf{n}) = \Omega_{\text{GW}}^{NS}(f, \mathbf{n}) + \Omega_{\text{GW}}^S(f, \mathbf{n}). \quad (4.2)$$

In the definition (4.2) the suffix *NS* indicates what we dub *non-stochastic part* of the spectrum, associated with anisotropies that are kinematically generated from the rest-frame monopole $\Omega'(f')$. The contribution with suffix *S* is the stochastic part of the spectrum, related with (stochastically-distributed) intrinsic anisotropies: this part experiences modulation and aberration effects due to the kinematic boost.

At first order in a β expansion, the only non-stochastic contribution is a dipole induced by the monopole, that reads

$$\Omega_{\text{GW}}^{NS}(f, \hat{\mathbf{n}}) = \sqrt{\frac{4\pi}{3}} \beta (4 - n_\Omega) \Omega'(f) Y_{10}(\hat{\mathbf{n}}), \quad (4.3)$$

where $\Omega'(f)$ is the quantity appearing in eq (4.1). Notice that the overall coefficient in eq (4.3) depends explicitly on n_Ω .

The stochastic part of the spectrum in the frame \mathcal{S} can be obtained from eq (2.22), which we rewrite in a slightly different form that is more convenient for our present purposes:

$$\Omega_{\text{GW}}^S(f, \hat{\mathbf{n}}) = (1 + \beta(4 - n_\Omega)\xi) [\Omega'_{\text{GW}}(f', \hat{\mathbf{n}}') - \beta(\nabla_a \xi) \nabla^a \Omega'_{\text{GW}}(f', \hat{\mathbf{n}}')] . \quad (4.4)$$

This expression makes manifest the (overall) effects of modulation, and the effects of aberration in the covariant derivatives of Ω'_{GW} .

With these tools we can compute correlations among stochastic anisotropies. It is convenient to expand the stochastic contributions to the spectrum in spherical harmonics

$$\Omega_{\text{GW}}^S(f, \hat{\mathbf{n}}) = \sum_{\ell m} \Omega_{\ell m}(f) Y_{\ell m}(\hat{\mathbf{n}}), \quad \Omega'_{\text{GW}}(f, \mathbf{n}) = \sum_{\ell m} \Omega'_{\ell m}(f) Y_{\ell m}(\hat{\mathbf{n}}). \quad (4.5)$$

Moreover, we also expand in dipolar harmonics the parameter $\xi(\hat{\mathbf{n}})$ of eq (2.2) and also

$$\beta \xi(\hat{\mathbf{n}}) = \sum_m Y_{1m}(\hat{\mathbf{n}}) \beta_{1m}. \quad (4.6)$$

Plugging these expansions eq (4.4), after standard manipulations (see also appendix A), one obtains at linear order in β the following relation among coefficients,

$$\Omega_{\ell m} = \Omega'_{\ell m} + \sum_{\ell_1 m_1 m_2} \left[3 - n_\Omega - \frac{\ell_1}{2}(\ell_1 + 1) + \frac{\ell}{2}(\ell + 1) \right] \Omega'_{\ell_1 m_1} \beta_{1 m_2} \mathcal{W}_{\ell \ell_1 1}^{m m_1 m_2}. \quad (4.7)$$

In writing this formula we introduced the Wigner-like symbol (see appendix A)

$$\mathcal{W}_{\ell_1 \ell_2 \ell_3}^{m_1 m_2 m_3} = \int d^2 n Y_{\ell_1 m_1}^* Y_{\ell_2 m_2} Y_{\ell_3 m_3}. \quad (4.8)$$

Since a boost violates statistical isotropy, the correlation functions among the $\Omega_{\ell m}$ of eq (4.7) can have a non-diagonal structure. We denote such correlations by a four-index quantity $F_{\ell m}^{\ell' m'}$ as

$$F_{\ell m}^{\ell' m'} \equiv \langle \Omega_{\ell m} \Omega_{\ell' m'} \rangle. \quad (4.9)$$

We conveniently split (4.9) into a statistically isotropic contribution, and a boost-induced contribution as

$$F_{\ell m}^{\ell' m'} = \delta_{\ell\ell'} \delta_{mm'} C_\ell + (F_{\ell m}^{\ell' m'})^\beta. \quad (4.10)$$

The boost-induced part – which violates statistical isotropy – is given by

$$(F_{\ell m}^{\ell' m'})^\beta = \beta_1 (m-m') [(3 - n_\Omega) (C_\ell + C_{\ell'}) + \alpha_{\ell\ell'} (C_\ell - C_{\ell'})] \mathcal{W}_{\ell \ell' 1}^{m m' m-m'}, \quad (4.11)$$

where

$$\alpha_{\ell\ell'} \equiv \frac{\ell'}{2}(\ell' + 1) - \frac{\ell}{2}(\ell + 1). \quad (4.12)$$

We notice that the result depends on the spectral tilt n_Ω : all the diagonal terms (i.e. $\ell = \ell', m = m'$) of the correlation matrices $(F_{\ell m}^{\ell' m'})^\beta$ are vanishing. Off-diagonal correlators are non-vanishing only for $\ell' = \ell \pm 1$, i.e. we have only correlation among $\ell \leftrightarrow \ell \pm 1$ multipoles. This is the consequence of the effect explained after eq (2.27): implementing a spherical-harmonic expansion of the density parameter, kinematic aberrations introduce contaminations between different multipoles. This result can be extended beyond linear order in β : at a generic order n th in the β -perturbation expansion in β (i.e. order β^n), only off-diagonal elements separated at most by n in multipole index are turned on. We plot the correlation (4.11) in Fig. 4 for two simple case studies.

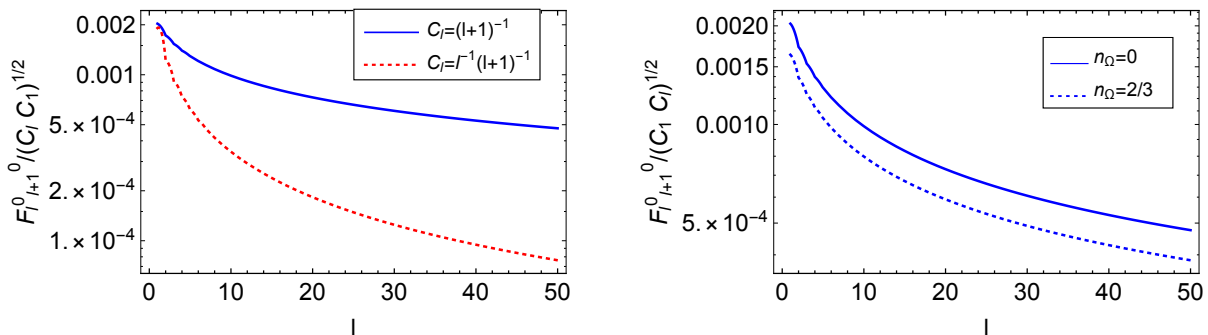


Figure 4: Left: The first off diagonal term of the correlation function (4.11), as function of ℓ . We choose $n_\Omega = 0$ and we test two different scalings of the intrinsic spectrum in eq. (4.11). Right: Same figure for two different values of n_Ω and for the astrophysically-motivated scaling of the left panel. In both panels the normalisation has been chosen for future convenience.

4.2 Fisher forecasts

We now develop Fisher forecasts for measuring the spectral tilt n_Ω , exploiting the properties of boost-induced anisotropies. We assume that the size of n_Ω is not too large, so that the dipole amplitude dominates over the quadrupole in a perturbative expansion of the non-stochastic term (4.3). Hence we consider only terms linear in boost velocity: this approximation is well justified as long as $\beta n_\Omega \ll 1$. The likelihood for the $\Omega_{\ell m}$ is assumed to be of the standard multivariate Gaussian form:

$$\ln \mathcal{L} = -\frac{1}{2} \left[\sum_{\ell m} \sum_{\ell' m'} (\Omega_{\ell m}^* - \Omega_{\ell m}^{NS*}) (F^{-1})_{\ell m}^{\ell' m'} (\Omega_{\ell' m'} - \Omega_{\ell' m'}^{NS}) + \ln \det (F)_{\ell m}^{\ell' m'} \right] + \text{const}. \quad (4.13)$$

We stress that the non-stochastic anisotropies $\Omega_{\ell' m'}^{NS}$ induced by the monopole are not inherently random. For this reason we treat them as a mean value. The covariance matrix is given by the two-point correlation function (4.11). To simplify our notation, we introduce the following matrix form

$$F_{\mu\nu} \equiv F_{\ell' m'}^{\ell' m'}, \quad (4.14)$$

where the first index corresponds to $\mu \equiv (\ell, m)$, while the second to $\nu \equiv (\ell', m')$. Calling δF the specific contribution of boost-induced anisotropies, we write ⁸

$$F_{\mu\nu} = \delta_{\mu\nu} C_\mu + \delta F_{\mu\nu}, \quad (4.15)$$

The theoretical covariance matrix $F_{\mu\nu}^{-1}$ generally depends on cosmological and astrophysical parameters λ_A . The uncertainty associated with these parameters is given by the Fisher matrix

$$\mathcal{F}_{AB} = \left\langle -\frac{\partial^2 \ln \mathcal{L}}{\partial \lambda_A \partial \lambda_B} \right\rangle, \quad (4.16)$$

which can be written more explicitly as (we use the shortcut notation $\partial_A \equiv \partial/\partial \lambda_A$)

$$\mathcal{F}_{AB} = \frac{1}{2} \sum_{\mu\nu\alpha\sigma} [(F^{-1})_{\mu\nu} \partial_A F_{\nu\sigma} (F^{-1})_{\sigma\alpha} \partial_B F_{\alpha\mu}] + \sum_{\mu\nu} \partial_A \Omega_\mu^{NS*} (F^{-1})_{\mu\nu} \partial_B \Omega_\nu^{NS}. \quad (4.17)$$

We start considering a perfect experiment with no instrumental noise, and we assume that the boost velocity is the same as the one measured by CMB experiments. We then discuss in a second step how the instrumental noise can be effectively included in the forecasts.

4.2.1 Uncertainty on the reconstruction of n_Ω

We now forecast the precision associated with the measurement of the spectral index parameter n_Ω controlling the amplitude of the boost-induced anisotropies. We assume that n_Ω is constant and it is the only free parameter to measure: a more realistic analysis would vary also other model parameters, but our specific goal in this context is to investigate whether the tilt n_Ω is detectable in the most favourable setting.

In this case the Fisher matrix has only one element

$$\mathcal{F}_{n_\Omega n_\Omega} = \sigma_{n_\Omega}^{-2} = \sum_\nu \frac{\partial \Omega_\nu^{NS*}}{\partial n_\Omega} (F^{-1})_\nu^\nu \frac{\partial \Omega_\nu^{NS}}{\partial n_\Omega} \delta_{\nu(1m)} + \frac{1}{2} \sum_\mu T_\mu. \quad (4.18)$$

The first term in this formula is associated with the non stochastic contributions given by eq. (4.3). We only keep the dipole, being the only contribution linear in β , and this explains the Kronecker symbol $\delta_{\nu(1m)}$. The second term of eq (4.18) is given by

$$T_\mu \equiv \sum_{\nu\sigma\rho} \delta C_{\mu\nu} (F^{-1})_{\nu\sigma} \delta C_{\sigma\rho} (F^{-1})_{\rho\mu}, \quad (4.19)$$

where with $\delta C_{\mu\nu}$ we denote the part of the correlation function (4.11) proportional to n_Ω :

$$\delta C_{\mu\nu} \equiv \frac{\partial \delta F_{\mu\nu}}{\partial n_\Omega}. \quad (4.20)$$

⁸With slight abuse of notation, we denote $C_\mu \equiv C_\ell$, although this quantity does not depend on the index m .

Notice that the non-stochastic anisotropies Ω_μ^{NS} given in eq. (4.3) *do* contribute to this formula, as they do depend on n_Ω . Since we expect the off-diagonal component to be suppressed relative to the diagonal one, we write

$$\begin{aligned} F_{\mu\nu} &= \sqrt{F_{\mu\mu}}\sqrt{F_{\nu\nu}} \left(\delta_{\mu\nu} + \frac{\delta F_{\mu\nu}}{\sqrt{F_{\mu\mu}}\sqrt{F_{\nu\nu}}} \right) \\ &= \sqrt{C_\mu}\sqrt{C_\nu} (\delta_{\mu\nu} + \epsilon_{\mu\nu}), \end{aligned} \quad (4.21)$$

using the relation $F_{\mu\mu} = C_\mu$. For the inverse of this quantity we find

$$(F^{-1})_{\mu\nu} \simeq \frac{\delta_{\mu\nu}}{C_\mu} - \frac{\delta F_{\mu\nu}}{C_\mu C_\nu}, \quad (4.22)$$

which gives for (4.19)

$$T_\mu \approx \frac{1}{C_\mu} \sum_\nu \frac{\delta C_{\mu\nu} \delta C_{\nu\mu}}{C_\nu} + \dots, \quad (4.23)$$

where terms of order $\sim (\delta C)^2 \delta F / C^3$ are neglected.

We now compute the contribution from the μ -dependent term, to understand how the different terms in the Fisher matrix contribute to the precision with which n_Ω can be reconstructed, i.e. $\sigma_{n_\Omega}^{-2}$ defined in (4.18). Going back to the usual notation $(\mu) = (\ell, m)$

$$(\sigma_{n_\Omega}^{-2})_{\ell m} = \frac{1}{C_\ell} \left[\sum_{\ell' m'} \frac{(\delta C)_{\ell m}^{\ell' m'} (\delta C)_{\ell' m'}^{\ell m}}{2C_{\ell'}} \right] + \delta_{\ell 1} \frac{1}{C_1} (\partial_{n_\Omega} \Omega_{1m}^{NS*}) (\partial_{n_\Omega} \Omega_{1m}^{NS}) + \mathcal{O}(\beta^3). \quad (4.24)$$

This expression is determined in terms of the multipoles in eq. (4.3), the correlation matrix in eq. (4.11), and the non-stochastic dipole (4.3).

Without loss of generality, we can choose a system of coordinates with azimuth aligned with e_z , where e_z denotes the direction of the boost velocity.⁹ In such a reference frame $m = m' = 0$. Moreover, the sum in (4.24) can be further simplified recalling that only multipoles with $(\ell - \ell') = \pm 1$ are correlated. We then obtain, using eq. (4.3),

$$(\sigma_{n_\Omega}^{-2})_\ell = \frac{\beta^2}{C_\ell} \left[\frac{(C_\ell + C_{\ell+1})^2}{2C_{\ell+1}} (\mathcal{W}_{\ell \ell+1}^{00 \ 0})^2 + \frac{(C_\ell + C_{\ell-1})^2}{2C_{\ell-1}} (\mathcal{W}_{\ell \ell-1}^{00 \ 0})^2 \right], \quad \ell > 1 \quad (4.25)$$

$$(\sigma_{n_\Omega}^{-2})_1 = \frac{\beta^2}{C_1} \left[\frac{(C_1 + C_2)^2}{2C_2} (\mathcal{W}_{12}^{00 \ 0})^2 \right] + \frac{4\pi}{3C_1} \beta^2 (\Omega'(f))^2. \quad (4.26)$$

This result confirms that, at leading order in β , non-stochastic anisotropies contribute only to the dipole through the last term in eq. (4.26). Hence, when considering an instrument with angular resolution ℓ , the corresponding uncertainty on the spectral tilt n_Ω is given by

$$\sigma_{n_\Omega} = \left[\sum_{\ell'=1}^{\ell} (\sigma_{n_\Omega}^{-2})_{\ell'} \right]^{-1/2}. \quad (4.27)$$

⁹To generalize our analysis, we can consider a rotated coordinate frame. The rotation is described by a SO(3) matrix R_1 characterized by its Euler angles $(\varphi_1, \theta_1, 0)$. In the new coordinate frame the boost direction is described by the unit vector $n_1 = R_1 e_z$. A direction described by a unit vector n in the old reference frame, is rotated to $R^{-1} n$ in the new one. The change to the rotated coordinate system does not change the results, however, and for the Fisher matrix analysis we will continue to use the preferred reference frame in which only the $m = 0$ component of the boost potential is non-zero.

We stress that until now we assumed that instrumental noise is negligible, and we only considered effects of cosmic variance. The contribution of instrumental noise can be taken into account replacing $C_\ell \rightarrow C_\ell + N_\ell$ in the denominator of (4.24), where N_ℓ is an estimate of instrumental noise per multipole for a given detector network, see e.g. [100].

4.2.2 Constraining the velocity β

We now assume that from the study of the monopole, we have a good reconstruction of the spectral index n_Ω in a given frequency band. We ask ourself the questions: can kinematic anisotropies be used to set constraints on the velocity of our relative motion with respect to the *emission* rest frame?

We assume that β is constant and it is the only free parameter to measure: a more realistic analysis would vary also other model parameters, but our specific goal in this context is to investigate whether β can be constrained in the most favourable setting.

By repeating steps totally analogous to what done in the previous section, one finds that the variance associate to β is given by

$$(\sigma_\beta^{-2})_\ell = [(3 - n_\Omega)(C_\ell + C_{\ell+1}) + (\ell + 1)(C_\ell - C_{\ell+1})]^2 \frac{(\mathcal{W}_{\ell \ell+1}^{00 \ 0})^2}{2C_{\ell+1}C_\ell} + \\ + [(3 - n_\Omega)(C_\ell + C_{\ell-1}) - \ell(C_\ell - C_{\ell-1})]^2 \frac{(\mathcal{W}_{\ell \ell-1}^{00 \ 0})^2}{2C_{\ell-1}C_\ell}, \quad \ell > 1, \quad (4.28)$$

$$(\sigma_{n_\Omega}^{-2})_1 = [(3 - n_\Omega)(C_1 + C_2) + 2(C_1 - C_2)]^2 \frac{(\mathcal{W}_{12}^{00 \ 0})^2}{2C_2C_1} + \frac{4\pi}{3C_1}(4 - n_\Omega)^2 \Omega'(f)^2. \quad (4.29)$$

The contribution of instrumental noise can be taken into account replacing $C_\ell \rightarrow C_\ell + N_\ell$ in the denominator of (4.28), where N_ℓ is an estimate of instrumental noise per multipole for a given detector network, see e.g. [100].

4.2.3 Signal-to-noise ratio of boost-induced anisotropies

We now compute the cumulative SNR associated with measurements of boost-induced anisotropies. To do so, we introduce a book-keeping parameter A controlling the amplitude of boost induced anisotropies, and send $\beta \rightarrow \beta A$. Then by definition

$$\mathcal{F}_{AA} = \sigma_A^{-2} = (S/N)^2 = \frac{1}{2} \sum_\mu P_\mu + \Omega_\nu^{NS*} (F^{-1})_\nu^\mu \Omega_\nu^{NS} \delta_{\nu(1m)}. \quad (4.30)$$

where the index A corresponds to the aforementioned book-keeping parameter relative to boost-induced quantities. We denote

$$P_\mu \equiv \sum_{\nu\sigma\rho} \delta F_{\mu\nu} (F^{-1})_{\nu\sigma} \delta F_{\sigma\rho} (F^{-1})_{\rho\mu}, \quad (4.31)$$

where δF is defined in (4.15). Eq. (4.31) can be approximated as

$$P_\mu \approx \frac{1}{C_\mu} \sum_\nu \frac{\delta F_{\mu\nu} \delta F_{\nu\mu}}{C_\nu} + \dots, \quad (4.32)$$

where we use (4.22) and as above we neglect terms of order $\sim (\delta F)^3/C^3$ and higher. Then

$$(S/N)_{\ell m}^2 = \frac{1}{C_\ell} \left[\sum_{\ell' m'} \frac{(\delta F)_{\ell m}^{\ell' m'} (\delta F)_{\ell' m'}^{\ell m}}{2C_{\ell'}} \right] + \delta_{\ell 1} \frac{1}{C_1} (\partial_A \Omega_{1m}^{NS*}) (\partial_A \Omega_{1m}^{NS}) + \mathcal{O}(\beta^3). \quad (4.33)$$

In our reference frame, $m = m' = 0$. Recalling that only multipoles $(\ell - \ell') = \pm 1$ correlate, (4.33) can be written as

$$\begin{aligned} (S/N)_\ell^2 &= \frac{\beta^2}{2C_\ell C_{\ell+1}} [(3 - n_\Omega)^2 (C_\ell + C_{\ell+1})^2 + (\ell + 1)^2 (C_\ell - C_{\ell+1})^2] (\mathcal{W}_{\ell \ell+1}^{00} \begin{smallmatrix} 0 \\ 1 \end{smallmatrix})^2 \\ &\quad + \frac{\beta^2}{2C_\ell C_{\ell-1}} [(3 - n_\Omega)^2 (C_\ell + C_{\ell-1})^2 + \ell^2 (C_\ell - C_{\ell-1})^2] (\mathcal{W}_{\ell \ell-1}^{00} \begin{smallmatrix} 0 \\ 1 \end{smallmatrix})^2 \\ (S/N)_1^2 &= \frac{\beta^2}{2C_1 C_2} [(3 - n_\Omega)^2 (C_1 + C_2)^2 + 4(C_1 - C_2)^2] (\mathcal{W}_{12}^{00} \begin{smallmatrix} 0 \\ 1 \end{smallmatrix})^2 + \frac{4\pi}{3C_1} \beta^2 (4 - n_\Omega)^2 (\Omega'(f))^2, \end{aligned} \quad (4.34)$$

where we used eq. (4.3). The cumulative SNR is given by

$$\left(\frac{S}{N} \right)_\ell^{\text{Cum}} = \sqrt{\sum_{\ell'=1}^{\ell} \left(\frac{S}{N} \right)_{\ell'}^2}. \quad (4.35)$$

We stress that up to now we assume to work in a cosmic-variance limited regime. However, as mentioned above, a contribution of instrumental noise can be included in (4.33) replacing the denominator with $C_\ell \rightarrow C_\ell + N_\ell$, where N_ℓ is an estimate of instrumental noise per multipole for a given detector network, see e.g. [100].

4.3 Illustration of the forecasting method: a case-study

As a practical illustration of the method, we apply our general results to a specific case study. We consider an astrophysical extra-galactic background of solar mass compact binaries with power spectral density with constant slope and $n_\Omega = 2/3$. As explained in section 3.2, for this case we expect the angular power spectrum to scale as the galaxy correlation function $\sim 1/(1 + \ell)$, and anisotropies to be suppressed with respect to the isotropic component of a typical factor $\sim (1 - 5) \times 10^{-2}$ depending on the astrophysical model. The astrophysical dependence of the angular power spectrum on the detail of the underlying astrophysical model has been studied in [26, 79–82, 87] and different formal aspects of the derivation of anisotropies and their interpretation are discussed in [58, 74, 83, 84, 87, 90].

We consider the most optimistic scenario in which the amplitude of the monopole is of the order of present upper bounds in the Hz band, $\bar{\Omega}_{\text{GW}}(f = 25\text{Hz}) \sim 3.4 \times 10^{-9}$ [4] and the angular power spectrum is suppressed with respect to monopole by a factor $10^{-3}/(\ell + 1)$. For a given detector network, the instrumental noise curve per multipole, N_ℓ , can be obtained using results of [100] and the publicly available code *schNell*¹⁰.

For illustrative purposes we consider:

¹⁰<https://github.com/damonge/schNell>

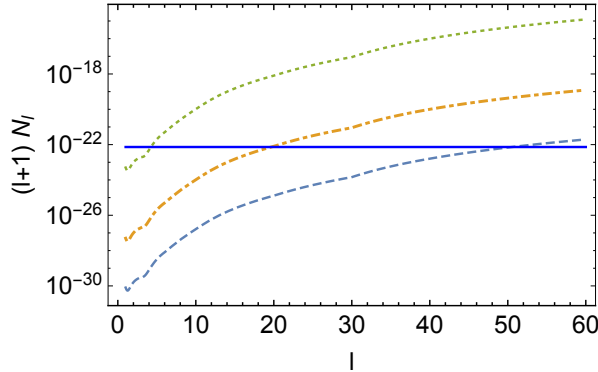


Figure 5: Instrumental noise per multipole for CE+ET and for two futuristic scenarios where the network detectors improve their strain sensitivity of a factor 10 and of a factor 50 respectively. We choose an integration time $T = 1$ year and $f = 63$ Hz. The blue line is the expected amplitude of a signal from a population of binary systems of stellar mass black holes, whose monopole is on the edge of being detected. The signal is time-independent while the noise decreases linearly with observation time [100]. The size of the non-stochastic dipole is $\sim 10^{-21}$.

- 1) a network made of Cosmic Explorer [101] plus Einstein Telescope [102], together with two futuristic scenarios where
- 2) both these instruments have an improvement in strain sensitivity of a factor 10 and
- 3) of a factor 50 with respect to their nominal values.

The instrumental noise per multipole in each of these three scenarios is plotted in Fig. 5 for a pivot frequency of 63 Hz, compared with the typical amplitude of the signal associated to an extra-galactic background at this frequency (clustering component).

In Fig. 6 we represent the expected (cumulative) precision for constraining the spectral density n_Ω in each one of the scenarios under study, as a function of multipole ℓ . We show separately what can be achieved using stochastic anisotropies only (left panel), and adding the non-stochastic dipole (right panel). In the right panel, we notice that the non-stochastic dipole sets the size of the error bar and stochastic anisotropies help to decrease the error when adding the contribution of very small angular scales. In this right panel we also see that all the three scenarios give the same result up to small angular scales (relative uncertainty of the order of 16%): the reason is that the stochastic dipole is well above the corresponding instrumental noise level, see Fig. 5. Hence cosmic variance is the dominant source of uncertainty in the determination of the dipole.

In Fig. 7 we represent the expected (cumulative) precision for constraining the velocity β in each one of the scenarios under study, as a function of multipole ℓ . We show separately what can be achieved using stochastic anisotropies only (left panel), and adding the non-stochastic dipole (right panel). Also in this case, we notice that the non-stochastic dipole sets the size of the error bars. The three scenarios give the same result up to small angular scales, with a relative uncertainty of the order of 30%.

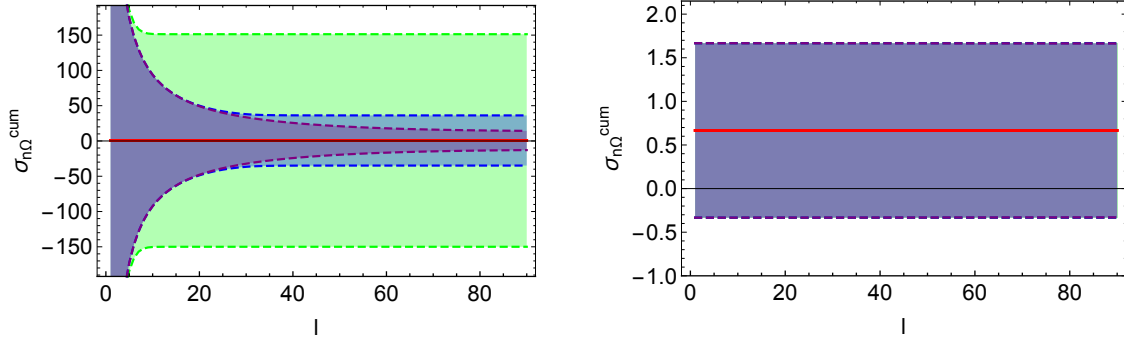


Figure 6: Variance on n_Ω as function of angular resolution. The red line represents the value of the spectral index $n_\Omega = 2/3$. The shaded green, blue and purple areas correspond to the 1σ region for the realistic scenario CE+ET and for the two futuristic scenarios described in the text (improvement in strain sensitivity of a factor 10 and 50 respectively). In the left panel we consider only the contribution of stochastic anisotropies, in the right one we also add the contribution from the non-stochastic dipole that plays an important role in controlling the error bars. The curves are indistinguishable up to very high multipoles, where the contribution of the stochastic component starts to be visible. We assume an integration time $T = 10$ years.

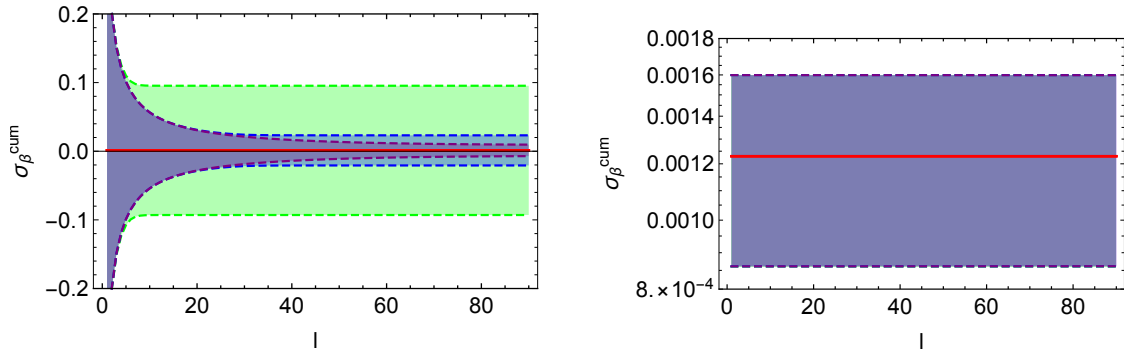


Figure 7: Variance on β as function of angular resolution. The red line represents the value of the velocity reconstructed from CMB experiments. The shaded green, blue and purple areas correspond to the 1σ region for the realistic scenario CE+ET and for the two futuristic scenarios described in the text (improvement in strain sensitivity of a factor 10 and 50 respectively). In the left panel we consider only the contribution of stochastic anisotropies, in the right one we also add the contribution from the non-stochastic dipole that plays an important role in controlling the error bars. The curves are indistinguishable up to very high multipoles, where the contribution of the stochastic component starts to be visible. We assume an integration time $T = 10$ years.

In Fig. 8 we show results for the cumulative SNR as a function of multipole, for each of the three scenarios under study. Also in this case, we plot separately the SNR associated to stochastic anisotropies alone, and then we add the contribution from the non-stochastic dipole (dashed lines). Each solid line reaches a plateau in correspondence to the angular scale at which the size of the signal in figure 5 reduces below the instrumental noise level. In this case too we notice that the non-stochastic dipole gives the dominant contribution to the cumulative signal to noise, up to very high multipoles, and that stochastic boost-induced anisotropies are not

detectable alone in the realistic CE+ET scenario.

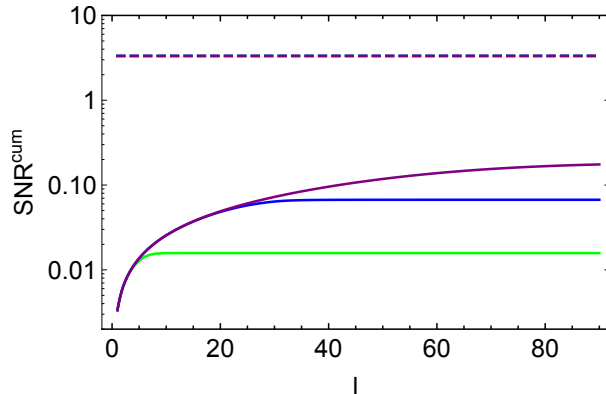


Figure 8: Cumulative SNR for the three scenarios described in the text (the color code is the same as for figure 6). With a solid line we represent the cumulative SNR associated to non-stochastic anisotropies, the dashed line also includes the contribution from the non-stochastic dipole, which dominates up to very small angular scales (the results for the three models are overlapped). We assume an integration time $T = 10$ years.

We stress that this analysis has only the scope of illustrating our forecasting method. A realistic study of the detectability of the spectral density for an astrophysical background in the Hz band should include a more realistic noise and signal description, e.g. taking into account a contribution from shot noise [79, 85, 86, 90], and deviations from the simple power law behaviour in the spectral index due to the merging phase of the evolution of binaries, see e.g. [79]. A similar analysis can be done on the cross-correlation between the background energy density and the distribution of galaxies which, for an astrophysical background, is expected to have an higher SNR than the auto-correlation – see e.g. [79, 81, 90, 93].

5 Outlook

In this paper we studied kinematic effects associated with the observer peculiar velocity on the energy density of the SGWB, paying special attention to their dependence on the frequency slope of the GW spectrum. We showed that a Doppler boost is responsible for the modulation and aberration of intrinsic anisotropies, and it additionally generates kinematic anisotropies from the rest-frame monopole of the SGWB. We provided analytic and ready-to-use expressions describing aberration, modulation and monopole-induced Doppler anisotropies of the SGWB. We showed that these effects are enhanced in the presence of large tilts of the frequency spectrum, and examined explicit examples where these findings can be relevant. We point out that a detection of boost-induced anisotropies can provide a complementary measurement of the spectral shape. We outlined a method to forecast the precision with which the spectral shape can be measured by a given detector network. For illustrative purposes, we applied this method to a simple case study: an extragalactic background with spectral index $n_\Omega = 2/3$ induced by coalescing binaries detectable with ET+CE. In this simple case we find that the monopole-induced dipole will allow us to constrain the spectral shape with a precision of about 16%. Interestingly, one can take

a different perspective, and from the study of the kinematic dipole, try to extract information about our peculiar motion (with respect to the CMB rest frame), assuming that the spectral shape in a given frequency band is reconstructed via binning methods. We show that a study of kinematic anisotropies with ET+CE can allow one to constrain our peculiar velocity with respect to the CMB frame with a precision of 30%.

Our analysis can be further developed in different directions. First, our forecasting method, which we presented for the case of a power-law frequency dependence for Ω_{GW} , can be generalized and applied to any frequency profile. It would be interesting to carry on such generalization to SGWB of cosmological origin whose spectral index can have non-trivial dependence on frequencies. Moreover, while in section 4 we included only kinematic corrections at first order in the β -expansion, it would be interesting to extend it at second order in β , for better clarifying consequences of mixing among different multipoles. At second order in β , one can constrain additional parameters controlling the properties of the spectrum, as for example α_{Ω} which can be important for cosmological backgrounds (see e.g. Fig 1).

A reconstruction of the spectral shape is a precious tool to distinguish background components with different origins. Current reconstruction methods require a detection in multiple frequency bands (binning), via small-band searches, which are more challenging than the broad band searches currently implemented by the LIGO-Virgo collaboration, in particular if the signal has a steep spectral shape, with a small frequency bin dominating the total SNR budget. The method that we present in this work may allow one to extract information on the spectral shape without the need of multiple band reconstruction.

Finally, SGWB kinematic dipole is a new observable which depends on both the spectral shape and on the velocity with which we move with respect to the emission frame (traditionally identified with the CMB rest frame). This new observable provides us with an independent way of reconstructing our kinematic motion: studying it could potentially shed light on the existing discrepancy in the value of β reconstructed from CMB and from galaxy number counts (see e.g. [103] and references therein for a recent critical analysis). We hope to return to these topics soon.

Acknowledgments

It is a pleasure to thank Nicola Bartolo, Robert Caldwell, Raphael Flauger, Marco Peloso, Angelo Ricciardone and Lorenzo Sorbo for useful discussions. GC is funded by Swiss National Science Foundation (Ambizione Grant). GT is partially funded by the STFC grant ST/T000813/1.

A Products of spherical harmonics and the Gaunt coefficient

In this appendix we summarise some properties of integrals over products of three spherical harmonics, and associated quantities. It is based on appendix H of [98]. The key result is that the integral of three spin-weighted spherical harmonics can be written as

$$\int d\Omega {}_{s_1}Y_{\ell_1 m_1} {}_{s_2}Y_{\ell_2 m_2} {}_{s_3}Y_{\ell_3 m_3} =$$

$$= \sqrt{\frac{(2\ell_1 + 1)(2\ell_2 + 1)(2\ell_3 + 1)}{4\pi}} \begin{pmatrix} \ell_1 & \ell_2 & \ell_3 \\ -s_1 & -s_2 & -s_3 \end{pmatrix} \begin{pmatrix} \ell_1 & \ell_2 & \ell_3 \\ m_1 & m_2 & m_3 \end{pmatrix}. \quad (\text{A.1})$$

The $3-j$ symbols that appear in this expression satisfy the following properties

$$\begin{pmatrix} \ell_1 & \ell_2 & \ell_3 \\ m_1 & m_2 & m_3 \end{pmatrix} = \begin{pmatrix} \ell_2 & \ell_3 & \ell_1 \\ m_2 & m_3 & m_1 \end{pmatrix} = \begin{pmatrix} \ell_3 & \ell_1 & \ell_2 \\ m_3 & m_1 & m_2 \end{pmatrix} \quad (\text{A.2})$$

$$= (-)^{\ell_1 + \ell_2 + \ell_3} \begin{pmatrix} \ell_1 & \ell_3 & \ell_2 \\ m_1 & m_3 & m_2 \end{pmatrix} \quad (\text{A.3})$$

$$= (-)^{\ell_1 + \ell_2 + \ell_3} \begin{pmatrix} \ell_1 & \ell_2 & \ell_3 \\ -m_1 & -m_2 & -m_3 \end{pmatrix}. \quad (\text{A.4})$$

Specifically, they are identically zero whenever any of the following conditions are violated

$$m_1 + m_2 + m_3 = 0, \quad |\ell_i - \ell_j| \leq \ell_k \leq \ell_i + \ell_j, \quad \{i, j\} = \{1, 2, 3\}. \quad (\text{A.5})$$

Some important quantities that are used in this paper are defined as

$$\mathcal{W}_{\ell_1 \ell_2 \ell_3}^{m_1 m_2 m_3} \equiv \int d\Omega Y_{\ell_1 m_1}^* Y_{\ell_2 m_2} Y_{\ell_3 m_3}, \quad (\text{A.6})$$

This is effectively the Gaunt coefficient (up to the complex conjugation of the first spherical harmonic which leads to some sign changes). It is given by

$$\mathcal{W}_{\ell_1 \ell_2 \ell_3}^{m_1 m_2 m_3} = (-1)^{m_1} \begin{pmatrix} \ell_1 & \ell_2 & \ell_3 \\ -m_1 & m_2 & m_3 \end{pmatrix} \mathcal{F}_{\ell_1 \ell_2 \ell_3}, \quad (\text{A.7})$$

$$\mathcal{F}_{\ell_1 \ell_2} = \sqrt{\frac{(2\ell + 1)(2\ell_1 + 1)(2\ell_2 + 2)}{4\pi}} \begin{pmatrix} \ell & \ell_1 & \ell_2 \\ 0 & 0 & 0 \end{pmatrix}. \quad (\text{A.8})$$

Another useful relation is that

$$\mathcal{I}_{\ell_1 \ell_2 \ell_3}^{m_1 m_2 m_3} = \frac{1}{2} [l_3(\ell_3 + 1) - \ell_2(\ell_2 + 1) - \ell_1(\ell_1 + 1)] \mathcal{W}_{\ell_1 \ell_2 \ell_3}^{m_1 m_2 m_3}, \quad (\text{A.9})$$

where

$$\mathcal{I}_{\ell_1 \ell_2 \ell_3}^{m_1 m_2 m_3} \equiv \int d\Omega Y_{\ell_1 m_1}^* \nabla^a Y_{\ell_2 m_2} \nabla_a Y_{\ell_3 m_3}. \quad (\text{A.10})$$

B On the validity of the β expansion in section 3.1

In this Appendix we reconsider the model of section 3.1, to demonstrate the consistency of a β^2 truncation in the expansion as in formulas (2.16)-(2.18). In fact, given that the spectral tilts are large – see Fig 1 – we should be cautious, and check whether contributions weighted by higher powers of β invalidate or not our formulas. We start from formula (2.12) and expand up fourth order in a β expansion. We obtain the following generalization of eqs (2.16)-(2.18):

$$M(f) = \frac{\beta^2}{6} (8 + n_\Omega (n_\Omega - 6) + \alpha_\Omega) + \frac{\beta^4}{24} (2n_\Omega^3 - 23n_\Omega^2 - 23\alpha_\Omega + 94n_\Omega + 6\alpha_\Omega n_\Omega + 2\gamma_\Omega - 136), \quad (\text{B.1})$$

$$D(f) = \beta (4 - n_\Omega) + \beta^3 \left(4n_\Omega - 8 - \frac{n_\Omega^2}{2} - \frac{\alpha_\Omega}{2} \right), \quad (\text{B.2})$$

$$Q(f) = \beta^2 \left(10 - \frac{9n_\Omega}{2} + \frac{n_\Omega^2}{2} + \frac{\alpha_\Omega}{2} \right) + \frac{\beta^4}{4} (n_\Omega^3 - 13n_\Omega^2 - 13\alpha_\Omega + 56n_\Omega + 3\alpha_\Omega n_\Omega + \gamma_\Omega - 80), \quad (\text{B.3})$$

indicating respectively the monopole, dipole, quadrupole Doppler contributions expanded up to β^4 . We define $\gamma_\Omega \equiv d\alpha_\Omega/d \ln f$. The monopole and quadrupole are sensitive to the fourth power of β , the dipole to the third power only.

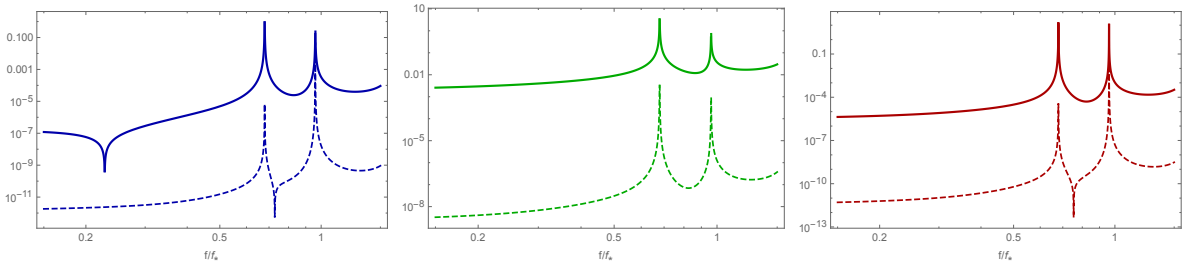


Figure 9: Kinematic contributions to the monopole ($M(f)$, left) dipole ($D(f)$, middle), and quadrupole ($Q(f)$, right) anisotropies, computed using formulas expanded up to order β^2 (continuous lines), together with the difference between their values computed up to order β^2 and up to order β^4 (dashed lines). We use the same values of parameters of Fig 2.

In Fig 9 we represent the frequency dependence of the kinematic anisotropies, computed using formulas expanded up to order β^2 in eqs (2.16)-(2.18), together with the difference between their values computed up to order β^2 and up to order β^4 using eqs (B.1)-(B.3). The difference is almost always orders of magnitude smaller than the kinematic anisotropies computed at order β^2 , except at the frequency $f/f_\star = 2/\sqrt{3}$. However, as explained in footnote 4, for that precise frequency resonant effects are expected to be smoothed out, at least in realistic situations. Hence, we conclude that the expansions used for making the plot in Fig 2 are sufficient for the values of the parameters chosen, and the results of section 3.1 are reliable.

References

- [1] T. Regimbau, “The astrophysical gravitational wave stochastic background,” *Res. Astron. Astrophys.* **11** (2011) 369–390, [arXiv:1101.2762 \[astro-ph.CO\]](#).
- [2] C. Caprini and D. G. Figueroa, “Cosmological Backgrounds of Gravitational Waves,” *Class. Quant. Grav.* **35** no. 16, (2018) 163001, [arXiv:1801.04268 \[astro-ph.CO\]](#).
- [3] M. Maggiore, *Gravitational Waves. Vol. 2: Astrophysics and Cosmology*. Oxford University Press, 2018.
- [4] **LIGO Scientific, Virgo, KAGRA** Collaboration, R. Abbott *et al.*, “Upper Limits on the Isotropic Gravitational-Wave Background from Advanced LIGO’s and Advanced Virgo’s Third Observing Run,” [arXiv:2101.12130 \[gr-qc\]](#).

- [5] **Virgo, LIGO Scientific** Collaboration, B. P. Abbott *et al.*, “Directional Limits on Persistent Gravitational Waves from Advanced LIGO’s First Observing Run,” *Phys. Rev. Lett.* **118** no. 12, (2017) 121102, [arXiv:1612.02030 \[gr-qc\]](#).
- [6] **LIGO Scientific, Virgo, KAGRA** Collaboration, R. Abbott *et al.*, “Search for anisotropic gravitational-wave backgrounds using data from Advanced LIGO’s and Advanced Virgo’s first three observing runs,” [arXiv:2103.08520 \[gr-qc\]](#).
- [7] **NANOGrav** Collaboration, Z. Arzoumanian *et al.*, “The NANOGrav 12.5 yr Data Set: Search for an Isotropic Stochastic Gravitational-wave Background,” *Astrophys. J. Lett.* **905** no. 2, (2020) L34, [arXiv:2009.04496 \[astro-ph.HE\]](#).
- [8] G. F. Smoot, M. V. Gorenstein, and R. A. Muller, “Detection of Anisotropy in the Cosmic Black Body Radiation,” *Phys. Rev. Lett.* **39** (1977) 898.
- [9] A. Kogut *et al.*, “Dipole anisotropy in the COBE DMR first year sky maps,” *Astrophys. J.* **419** (1993) 1, [arXiv:astro-ph/9312056 \[astro-ph\]](#).
- [10] **WMAP** Collaboration, C. L. Bennett *et al.*, “First year Wilkinson Microwave Anisotropy Probe (WMAP) observations: Preliminary maps and basic results,” *Astrophys. J. Suppl.* **148** (2003) 1–27, [arXiv:astro-ph/0302207 \[astro-ph\]](#).
- [11] **Planck** Collaboration, N. Aghanim *et al.*, “Planck 2013 results. XXVII. Doppler boosting of the CMB: Eppur si muove,” *Astron. Astrophys.* **571** (2014) A27, [arXiv:1303.5087 \[astro-ph.CO\]](#).
- [12] G. R. Henry, R. B. Feduniak, J. E. Silver, and M. A. Peterson, “Distribution of black body cavity radiation in a moving frame of reference,” *Phys. Rev.* **176** (1968) 1451–1455.
- [13] P. J. E. Peebles and D. T. Wilkinson, “Comment on the Anisotropy of the Primeval Fireball,” *Phys. Rev.* **174** (1968) 2168–2168.
- [14] K. M. Gorski, “Will COBE challenge the inflationary paradigm? 1. Cosmic microwave background anisotropies versus large scale streaming motions (Revised),” *Submitted to: Ap. J.(Letters) 1990 July XX* (1990) .
- [15] A. Challinor and F. van Leeuwen, “Peculiar velocity effects in high resolution microwave background experiments,” *Phys. Rev.* **D65** (2002) 103001, [arXiv:astro-ph/0112457 \[astro-ph\]](#).
- [16] D. Menzies and G. J. Mathews, “Peculiar velocity and deaberration of the sky,” *Astrophys. J.* **624** (2005) 7–9, [arXiv:astro-ph/0409175 \[astro-ph\]](#).
- [17] S. Burles and S. Rappaport, “Aberration of the Cosmic Microwave Background,” *Astrophys. J.* **641** (2006) L1, [arXiv:astro-ph/0601559 \[astro-ph\]](#).
- [18] A. Kosowsky and T. Kahniashvili, “The Signature of Proper Motion in the Microwave Sky,” *Phys. Rev. Lett.* **106** (2011) 191301, [arXiv:1007.4539 \[astro-ph.CO\]](#).

- [19] L. Amendola *et al.*, “Measuring our peculiar velocity on the CMB with high-multipole off-diagonal correlations,” *JCAP* **1107** (2011) 027, [arXiv:1008.1183 \[astro-ph.CO\]](#).
- [20] S. Mukherjee, A. De and T. Souradeep, “Statistical isotropy violation of CMB Polarization sky due to Lorentz boost,” [arXiv:1309.3800 \[astro-ph.CO\]](#).
- [21] C. Bonvin, R. Durrer, and M. Kunz, “The dipole of the luminosity distance: a direct measure of $H(z)$,” *Phys. Rev. Lett.* **96** (2006) 191302, [arXiv:astro-ph/0603240 \[astro-ph\]](#).
- [22] G. F. R. Ellis and J. E. Baldwin, “On the expected anisotropy of radio source counts,” *Monthly Notices of the Royal Astronomical Society* **206** no. 2, (01, 1984) 377–381.
- [23] R. Maartens, C. Clarkson, and S. Chen, “The kinematic dipole in galaxy redshift surveys,” *JCAP* **1801** (2018) 013, [arXiv:1709.04165 \[astro-ph.CO\]](#).
- [24] N. Pant, A. Rotti, C. A. P. Bengaly, and R. Maartens, “Measuring our velocity from fluctuations in number counts,” *JCAP* **1903** (2019) 023, [arXiv:1808.09743 \[astro-ph.CO\]](#).
- [25] N. Bartolo *et al.*, “Probing Anisotropies of the Stochastic Gravitational Wave Background with LISA,” [arXiv:2201.08782 \[astro-ph.CO\]](#).
- [26] A. C. Jenkins and M. Sakellariadou, “Anisotropies in the stochastic gravitational-wave background: Formalism and the cosmic string case,” *Phys. Rev.* **D98** no. 6, (2018) 063509, [arXiv:1802.06046 \[astro-ph.CO\]](#).
- [27] J. McKinley, “Relativistic transformations of light power,” *Am. J. Phys.* **47** (1979) 602.
- [28] L. D. Landau and E. M. Lifshitz, *Course of Theoretical Physics, Vol. II: Classical field theory*. 1987.
- [29] M. Kamionkowski and L. Knox, “Aspects of the cosmic microwave background dipole,” *Phys. Rev.* **D67** (2003) 063001, [arXiv:astro-ph/0210165 \[astro-ph\]](#).
- [30] B. Allen and A. C. Ottewill, “Detection of anisotropies in the gravitational wave stochastic background,” *Phys. Rev.* **D56** (1997) 545–563, [arXiv:gr-qc/9607068 \[gr-qc\]](#).
- [31] N. Bartolo *et al.*, “Science with the space-based interferometer LISA. IV: Probing inflation with gravitational waves,” *JCAP* **1612** (2016) 026, [arXiv:1610.06481 \[astro-ph.CO\]](#).
- [32] D. Cannone, G. Tasinato, and D. Wands, “Generalised tensor fluctuations and inflation,” *JCAP* **01** (2015) 029, [arXiv:1409.6568 \[astro-ph.CO\]](#).
- [33] N. Bartolo, D. Cannone, A. Ricciardone, and G. Tasinato, “Distinctive signatures of space-time diffeomorphism breaking in EFT of inflation,” *JCAP* **03** (2016) 044, [arXiv:1511.07414 \[astro-ph.CO\]](#).

- [34] A. Ricciardone and G. Tasinato, “Primordial gravitational waves in supersolid inflation,” *Phys. Rev. D* **96** no. 2, (2017) 023508, [arXiv:1611.04516 \[astro-ph.CO\]](#).
- [35] S. Matarrese, O. Pantano, and D. Saez, “A General relativistic approach to the nonlinear evolution of collisionless matter,” *Phys. Rev.* **D47** (1993) 1311–1323.
- [36] S. Matarrese, O. Pantano, and D. Saez, “General relativistic dynamics of irrotational dust: Cosmological implications,” *Phys. Rev. Lett.* **72** (1994) 320–323, [arXiv:astro-ph/9310036 \[astro-ph\]](#).
- [37] S. Matarrese, S. Mollerach, and M. Bruni, “Second order perturbations of the Einstein-de Sitter universe,” *Phys. Rev.* **D58** (1998) 043504, [arXiv:astro-ph/9707278 \[astro-ph\]](#).
- [38] H. Noh and J.-c. Hwang, “Second-order perturbations of the Friedmann world model,” *Phys. Rev.* **D69** (2004) 104011.
- [39] K. Nakamura, “Second-order gauge invariant cosmological perturbation theory: Einstein equations in terms of gauge invariant variables,” *Prog. Theor. Phys.* **117** (2007) 17–74, [arXiv:gr-qc/0605108 \[gr-qc\]](#).
- [40] K. N. Ananda, C. Clarkson, and D. Wands, “The Cosmological gravitational wave background from primordial density perturbations,” *Phys. Rev.* **D75** (2007) 123518, [arXiv:gr-qc/0612013 \[gr-qc\]](#).
- [41] D. Baumann, P. J. Steinhardt, K. Takahashi, and K. Ichiki, “Gravitational Wave Spectrum Induced by Primordial Scalar Perturbations,” *Phys. Rev.* **D76** (2007) 084019, [arXiv:hep-th/0703290 \[hep-th\]](#).
- [42] M. Sasaki, T. Suyama, T. Tanaka, and S. Yokoyama, “Primordial black holes? perspectives in gravitational wave astronomy,” *Classical and Quantum Gravity* **35** no. 6, (Feb, 2018) 063001. <http://dx.doi.org/10.1088/1361-6382/aaa7b4>.
- [43] B. Carr, F. Kühnel, and M. Sandstad, “Primordial black holes as dark matter,” *Physical Review D* **94** no. 8, (Oct, 2016) . <http://dx.doi.org/10.1103/PhysRevD.94.083504>.
- [44] R. Saito and J. Yokoyama, “Gravitational wave background as a probe of the primordial black hole abundance,” *Phys. Rev. Lett.* **102** (2009) 161101, [arXiv:0812.4339 \[astro-ph\]](#). [Erratum: *Phys. Rev. Lett.*107,069901(2011)].
- [45] R. Saito and J. Yokoyama, “Gravitational-Wave Constraints on the Abundance of Primordial Black Holes,” *Prog. Theor. Phys.* **123** (2010) 867–886, [arXiv:0912.5317 \[astro-ph.CO\]](#). [Erratum: *Prog. Theor. Phys.*126,351(2011)].
- [46] S. Pi and M. Sasaki, “Gravitational Waves Induced by Scalar Perturbations with a Lognormal Peak,” *JCAP* **2009** (2020) 037, [arXiv:2005.12306 \[gr-qc\]](#).
- [47] J. R. Espinosa, D. Racco, and A. Riotto, “A Cosmological Signature of the SM Higgs Instability: Gravitational Waves,” *JCAP* **1809** (2018) 012, [arXiv:1804.07732 \[hep-ph\]](#).

- [48] K. Kohri and T. Terada, “Semianalytic calculation of gravitational wave spectrum nonlinearly induced from primordial curvature perturbations,” *Phys. Rev.* **D97** no. 12, (2018) 123532, [arXiv:1804.08577 \[gr-qc\]](#).
- [49] M. Braglia, D. K. Hazra, F. Finelli, G. F. Smoot, L. Sriramkumar, and A. A. Starobinsky, “Generating PBHs and small-scale GWs in two-field models of inflation,” *JCAP* **2008** (2020) 001, [arXiv:2005.02895 \[astro-ph.CO\]](#).
- [50] S. Kuroyanagi, T. Chiba, and T. Takahashi, “Probing the Universe through the Stochastic Gravitational Wave Background,” *JCAP* **1811** (2018) 038, [arXiv:1807.00786 \[astro-ph.CO\]](#).
- [51] C. Caprini, D. G. Figueroa, R. Flauger, G. Nardini, M. Peloso, M. Pieroni, A. Ricciardone, and G. Tasinato, “Reconstructing the spectral shape of a stochastic gravitational wave background with LISA,” *JCAP* **1911** (2019) 017, [arXiv:1906.09244 \[astro-ph.CO\]](#).
- [52] R. Flauger, N. Karnesis, G. Nardini, M. Pieroni, A. Ricciardone, and J. Torrado, “Improved reconstruction of a stochastic gravitational wave background with LISA,” *JCAP* **2101** (2021) 059, [arXiv:2009.11845 \[astro-ph.CO\]](#).
- [53] R.-G. Cai, S. Pi, S.-J. Wang, and X.-Y. Yang, “Resonant multiple peaks in the induced gravitational waves,” *JCAP* **1905** (2019) 013, [arXiv:1901.10152 \[astro-ph.CO\]](#).
- [54] K. Inomata, K. Kohri, T. Nakama, and T. Terada, “Enhancement of Gravitational Waves Induced by Scalar Perturbations due to a Sudden Transition from an Early Matter Era to the Radiation Era,” *Phys. Rev.* **D100** no. 4, (2019) 043532, [arXiv:1904.12879 \[astro-ph.CO\]](#).
- [55] J. Fumagalli, S. Renaux-Petel, and L. T. Witkowski, “Oscillations in the stochastic gravitational wave background from sharp features and particle production during inflation,” [arXiv:2012.02761 \[astro-ph.CO\]](#).
- [56] J. Fumagalli, G. A. Palma, S. Renaux-Petel, S. Sypsas, L. T. Witkowski and C. Zenteno, “Primordial gravitational waves from excited states,” *JHEP* **03** (2022) 196, [arXiv:2111.14664 \[astro-ph.CO\]](#).
- [57] V. Alba and J. Maldacena, “Primordial gravity wave background anisotropies,” *JHEP* **03** (2016) 115, [arXiv:1512.01531 \[hep-th\]](#).
- [58] C. R. Contaldi, “Anisotropies of Gravitational Wave Backgrounds: A Line Of Sight Approach,” *Phys. Lett.* **B771** (2017) 9–12, [arXiv:1609.08168 \[astro-ph.CO\]](#).
- [59] D. Bertacca, A. Raccanelli, N. Bartolo, and S. Matarrese, “Cosmological perturbation effects on gravitational-wave luminosity distance estimates,” *Phys. Dark Univ.* **20** (2018) 32–40, [arXiv:1702.01750 \[gr-qc\]](#).

- [60] N. Bartolo, D. Bertacca, S. Matarrese, M. Peloso, A. Ricciardone, A. Riotto, and G. Tasinato, “Anisotropies and non-Gaussianity of the Cosmological Gravitational Wave Background,” *Phys. Rev.* **D100** no. 12, (2019) 121501, [arXiv:1908.00527](#) [[astro-ph.CO](#)].
- [61] N. Bartolo, D. Bertacca, V. De Luca, G. Franciolini, S. Matarrese, M. Peloso, A. Ricciardone, A. Riotto, and G. Tasinato, “Gravitational wave anisotropies from primordial black holes,” *JCAP* **2002** (2020) 028, [arXiv:1909.12619](#) [[astro-ph.CO](#)].
- [62] N. Bartolo, D. Bertacca, S. Matarrese, M. Peloso, A. Ricciardone, A. Riotto, and G. Tasinato, “Characterizing the cosmological gravitational wave background: Anisotropies and non-Gaussianity,” *Phys. Rev.* **D102** no. 2, (2020) 023527, [arXiv:1912.09433](#) [[astro-ph.CO](#)].
- [63] V. Domcke, R. Jinno, and H. Rubira, “Deformation of the gravitational wave spectrum by density perturbations,” *JCAP* **2006** (2020) 046, [arXiv:2002.11083](#) [[astro-ph.CO](#)].
- [64] L. Valbusa Dall’Armi, A. Ricciardone, N. Bartolo, D. Bertacca, and S. Matarrese, “Imprint of relativistic particles on the anisotropies of the stochastic gravitational-wave background,” *Phys. Rev.* **D103** no. 2, (2021) 023522, [arXiv:2007.01215](#) [[astro-ph.CO](#)].
- [65] E. Dimastrogiovanni, M. Fasiello, A. Malhotra, P. D. Meerburg, and G. Orlando, “Testing the Early Universe with Anisotropies of the Gravitational Wave Background,” [arXiv:2109.03077](#) [[astro-ph.CO](#)].
- [66] A. Ricciardone and G. Tasinato, “Anisotropic tensor power spectrum at interferometer scales induced by tensor squeezed non-Gaussianity,” *JCAP* **1802** (2018) 011, [arXiv:1711.02635](#) [[astro-ph.CO](#)].
- [67] E. Dimastrogiovanni, M. Fasiello, G. Tasinato, and D. Wands, “Tensor non-Gaussianities from Non-minimal Coupling to the Inflaton,” *JCAP* **1902** (2019) 008, [arXiv:1810.08866](#) [[astro-ph.CO](#)].
- [68] E. Dimastrogiovanni, M. Fasiello, and G. Tasinato, “Searching for Fossil Fields in the Gravity Sector,” *Phys. Rev. Lett.* **124** no. 6, (2020) 061302, [arXiv:1906.07204](#) [[astro-ph.CO](#)].
- [69] P. Adshead, N. Afshordi, E. Dimastrogiovanni, M. Fasiello, E. A. Lim, and G. Tasinato, “Multimessenger cosmology: Correlating cosmic microwave background and stochastic gravitational wave background measurements,” *Phys. Rev.* **D103** no. 2, (2021) 023532, [arXiv:2004.06619](#) [[astro-ph.CO](#)].
- [70] N. Seto, “Prospects for direct detection of circular polarization of gravitational-wave background,” *Phys. Rev. Lett.* **97** (2006) 151101, [arXiv:astro-ph/0609504](#) [[astro-ph](#)].
- [71] V. Domcke, J. Garcia-Bellido, M. Peloso, M. Pieroni, A. Ricciardone, L. Sorbo, and G. Tasinato, “Measuring the net circular polarization of the stochastic gravitational wave

- background with interferometers,” *JCAP* **2005** (2020) 028, [arXiv:1910.08052 \[astro-ph.CO\]](#).
- [72] M. Lewicki and V. Vaskonen, “Impact of LIGO-Virgo binaries on gravitational wave background searches,” [arXiv:2111.05847 \[astro-ph.CO\]](#).
- [73] P. A. Rosado, “Gravitational wave background from binary systems,” *Phys. Rev.* **D84** (2011) 084004, [arXiv:1106.5795 \[gr-qc\]](#).
- [74] C. Pitrou, G. Cusin, and J.-P. Uzan, “Unified view of anisotropies in the astrophysical gravitational-wave background,” *Phys. Rev. D* **101** no. 8, (2020) 081301, [arXiv:1910.04645 \[astro-ph.CO\]](#).
- [75] I. Dvorkin, J.-P. Uzan, E. Vangioni, and J. Silk, “Synthetic model of the gravitational wave background from evolving binary compact objects,” *Phys. Rev. D* **94** no. 10, (2016) 103011, [arXiv:1607.06818 \[astro-ph.HE\]](#).
- [76] **LIGO Scientific, Virgo** Collaboration, B. P. Abbott *et al.*, “GW170817: Observation of Gravitational Waves from a Binary Neutron Star Inspiral,” *Phys. Rev. Lett.* **119** no. 16, (2017) 161101, [arXiv:1710.05832 \[gr-qc\]](#).
- [77] **LIGO Scientific, Virgo** Collaboration, B. P. Abbott *et al.*, “GWTC-1: A Gravitational-Wave Transient Catalog of Compact Binary Mergers Observed by LIGO and Virgo during the First and Second Observing Runs,” *Phys. Rev. X* **9** no. 3, (2019) 031040, [arXiv:1811.12907 \[astro-ph.HE\]](#).
- [78] **LIGO Scientific, Virgo** Collaboration, B. P. Abbott *et al.*, “Search for the isotropic stochastic background using data from Advanced LIGOs second observing run,” *Phys. Rev.* **D100** no. 6, (2019) 061101, [arXiv:1903.02886 \[gr-qc\]](#).
- [79] G. Cusin, I. Dvorkin, C. Pitrou, and J.-P. Uzan, “Properties of the stochastic astrophysical gravitational wave background: astrophysical sources dependencies,” *Phys. Rev. D* **100** no. 6, (2019) 063004, [arXiv:1904.07797 \[astro-ph.CO\]](#).
- [80] G. Cusin, I. Dvorkin, C. Pitrou, and J.-P. Uzan, “Stochastic gravitational wave background anisotropies in the mHz band: astrophysical dependencies,” *Mon. Not. Roy. Astron. Soc.* **493** no. 1, (2020) L1–L5, [arXiv:1904.07757 \[astro-ph.CO\]](#).
- [81] G. Cusin, I. Dvorkin, C. Pitrou, and J.-P. Uzan, “First predictions of the angular power spectrum of the astrophysical gravitational wave background,” *Phys. Rev. Lett.* **120** (2018) 231101, [arXiv:1803.03236 \[astro-ph.CO\]](#).
- [82] A. C. Jenkins, M. Sakellariadou, T. Regimbau, and E. Slezak, “Anisotropies in the astrophysical gravitational-wave background: Predictions for the detection of compact binaries by LIGO and Virgo,” *Phys. Rev.* **D98** no. 6, (2018) 063501, [arXiv:1806.01718 \[astro-ph.CO\]](#).

- [83] G. Cusin, C. Pitrou, and J.-P. Uzan, “The signal of the gravitational wave background and the angular correlation of its energy density,” *Phys. Rev.* **D97** no. 12, (2018) 123527, [arXiv:1711.11345](#) [[astro-ph.CO](#)].
- [84] G. Cusin, C. Pitrou, and J.-P. Uzan, “Anisotropy of the astrophysical gravitational wave background: Analytic expression of the angular power spectrum and correlation with cosmological observations,” *Phys. Rev.* **D96** no. 10, (2017) 103019, [arXiv:1704.06184](#) [[astro-ph.CO](#)].
- [85] A. C. Jenkins and M. Sakellariadou, “Shot noise in the astrophysical gravitational-wave background,” [arXiv:1902.07719](#) [[astro-ph.CO](#)].
- [86] A. C. Jenkins, J. D. Romano, and M. Sakellariadou, “Estimating the angular power spectrum of the gravitational-wave background in the presence of shot noise,” [arXiv:1907.06642](#) [[astro-ph.CO](#)].
- [87] G. Cusin, R. Durrer, and P. G. Ferreira, “Polarization of a stochastic gravitational wave background through diffusion by massive structures,” *Phys. Rev. D* **99** no. 2, (2019) 023534, [arXiv:1807.10620](#) [[astro-ph.CO](#)].
- [88] D. Bertacca, A. Ricciardone, N. Bellomo, A. C. Jenkins, S. Matarrese, A. Raccanelli, T. Regimbau, and M. Sakellariadou, “Projection effects on the observed angular spectrum of the astrophysical stochastic gravitational wave background,” *Phys. Rev.* **D101** no. 10, (2020) 103513, [arXiv:1909.11627](#) [[astro-ph.CO](#)].
- [89] S. Mukherjee and J. Silk, “Time-dependence of the astrophysical stochastic gravitational wave background,” [arXiv:1912.07657](#) [[gr-qc](#)].
- [90] D. Alonso, G. Cusin, P. G. Ferreira, and C. Pitrou, “Detecting the anisotropic astrophysical gravitational wave background in the presence of shot noise through cross-correlations,” *Phys. Rev. D* **102** no. 2, (2020) 023002, [arXiv:2002.02888](#) [[astro-ph.CO](#)].
- [91] **LIGO Scientific, Virgo** Collaboration, B. P. Abbott *et al.*, “Directional limits on persistent gravitational waves using data from Advanced LIGO’s first two observing runs,” *Phys. Rev. D* **100** no. 6, (2019) 062001, [arXiv:1903.08844](#) [[gr-qc](#)].
- [92] J. Baker *et al.*, “High angular resolution gravitational wave astronomy,” [arXiv:1908.11410](#) [[astro-ph.HE](#)].
- [93] K. Z. Yang, V. Mandic, C. Scarlata, and S. Banagiri, “Searching for Cross-Correlation Between Stochastic Gravitational Wave Background and Galaxy Number Counts,” *Mon. Not. Roy. Astron. Soc.* **500** no. 2, (2020) 1666–1672, [arXiv:2007.10456](#) [[astro-ph.CO](#)].
- [94] A. Lamberts, S. Garrison-Kimmel, P. Hopkins, E. Quataert, J. Bullock, C.-A. Faucher-Giguere, A. Wetzel, D. Keres, K. Drango, and R. Sanderson, “Predicting the binary black hole population of the Milky Way with cosmological simulations,” *Mon. Not. Roy. Astron. Soc.* **480** no. 2, (2018) 2704–2718, [arXiv:1801.03099](#) [[astro-ph.GA](#)].

- [95] A. Lamberts, S. Blunt, T. B. Littenberg, S. Garrison-Kimmel, T. Kupfer, and R. E. Sanderson, “Predicting the LISA white dwarf binary population in the Milky Way with cosmological simulations,” *Mon. Not. Roy. Astron. Soc.* **490** no. 4, (2019) 5888–5903, [arXiv:1907.00014 \[astro-ph.HE\]](#).
- [96] T. Robson, N. Cornish, “Impact of galactic foreground characterization on a global analysis for the LISA gravitational wave observatory,” *Class. Quant. Grav.* **34** (2017) 244002, [arXiv:1705.09421 \[gr-qc\]](#).
- [97] S. Dodelson, *Modern Cosmology*. Academic Press, Amsterdam, 2003. <http://www.slac.stanford.edu/spires/find/books/www?cl=QB981:D62:2003>.
- [98] G. Cusin, C. Pitrou, and J.-P. Uzan, “Are we living near the center of a local void?,” *JCAP* **1703** no. 03, (2017) 038, [arXiv:1609.02061 \[astro-ph.CO\]](#).
- [99] V. Nistane, G. Cusin, and M. Kunz, “CMB sky for an off-center observer in a local void. Part I. Framework for forecasts,” *JCAP* **12** (2019) 038, [arXiv:1908.05484 \[astro-ph.CO\]](#).
- [100] D. Alonso, C. R. Contaldi, G. Cusin, P. G. Ferreira, and A. I. Renzini, “Noise angular power spectrum of gravitational wave background experiments,” *Phys. Rev. D* **101** no. 12, (2020) 124048, [arXiv:2005.03001 \[astro-ph.CO\]](#).
- [101] D. Reitze *et al.*, “Cosmic Explorer: The U.S. Contribution to Gravitational-Wave Astronomy beyond LIGO,” *Bull. Am. Astron. Soc.* **51** no. 7, (2019) 035, [arXiv:1907.04833 \[astro-ph.IM\]](#).
- [102] S. Hild, S. Chelkowski, and A. Freise, “Pushing towards the et sensitivity using ‘conventional’ technology,” 2008.
- [103] C. Dalang, C. Bonvin, “On the kinematic cosmic dipole tension”, [arXiv:2111.0361 \[astro-ph.CO\]](#).